Energy-Resolved Collision-Induced Dissociation Studies of 2,2 '-Bipyridine Complexes of the Late First-Row Divalent Transition-Metal Cations: Determination of the Third-Sequential...

ARTICLE *in* THE JOURNAL OF PHYSICAL CHEMISTRY A · APRIL 2013

Impact Factor: 2.69 · DOI: 10.1021/jp401711c · Source: PubMed

3 AUTHORS, INCLUDING:

Yu Chen
University of Illinois, Urbana-Champaign
20 PUBLICATIONS **147** CITATIONS
SEE PROFILE

Mary T Rodgers
Wayne State University
125 PUBLICATIONS **4,177** CITATIONS
SEE PROFILE

THE JOURNAL OF PHYSICAL CHEMISTRY A

Article

pubs.acs.org/JPCA

Energy-Resolved Collision-Induced Dissociation Studies of 1,10-Phenanthroline Complexes of the Late First-Row Divalent Transition Metal Cations: Determination of the Third Sequential Binding Energies

Holliness Nose, Yu Chen, and M. T. Rodgers*

Department of Chemistry, Wayne State University, Detroit, Michigan 48202, United States

Supporting Information

ABSTRACT: The third sequential binding energies of the late first-row divalent transition metal cations to 1,10-phenanthroline (Phen) are determined by energy-resolved collision-induced dissociation (CID) techniques using a guided ion beam tandem mass spectrometer. Five late first-row transition metal cations in their +2 oxidation states are examined including: Fe^{2+}, Co^{2+}, Ni^{2+}, Cu^{2+}, and Zn^{2+}. The kinetic energy dependent CID cross sections for loss of an intact Phen ligand from the $M^{2+}(Phen)_3$ complexes are modeled to obtain 0 and 298 K bond dissociation energies (BDEs) after accounting for the effects of the internal energy of the complexes, multiple ion−neutral collisions, and unimolecular decay rates. Electronic structure theory calculations at the B3LYP, BHandHLYP, and M06 levels of theory are employed to determine the structures and theoretical estimates for the first, second, and third sequential BDEs of the $M^{2+}(Phen)_x$ complexes. B3LYP was found to deliver results that are most consistent with the measured values. Periodic trends in the binding of these complexes are examined and compared to the analogous complexes to the late first-row monovalent transition metal cations, Co^+, Ni^+, Cu^+, and Zn^+, previously investigated.

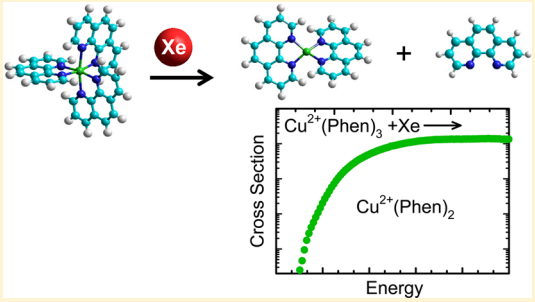

INTRODUCTION

Transition metal coordination complexes (TMCCs) are a very diverse and important class of molecules due to the variation in electronic and geometric structures they exhibit as a function of the local chemical environment. TMCCs can be sterically and electronically tuned by appropriate choice of the metal center and by manipulating the type, structure, and number of ligands.[1,2] Bulky ligands exert steric effects on the metal center and may influence catalytic activity by changing the geometry of the complex and controlling accessibility to the metal center. 1,10-Phenanthroline (Phen) is a bulky ligand and a strong chelator to a variety of transition metals.[3−6] Therefore, transition metal−Phen complexes have become attractive templates as Lewis acid binding sites and catalysts.[7−10] Substituted Phen ligands have found widespread use in asymmetric catalysis.[11−13] The rigidity of the Phen core helps stabilize favorable TMCCs and translates their chiral information with greater fidelity during catalysis. TMCCs exhibit advantages over main group Lewis acid catalysts. Their occupied d orbitals, which main group Lewis acids do not possess, offer unique electronic properties and a greater number of possible geometries to influence the binding and activation of molecules.[14] TMCCs also often lack the problems of water sensitivity and potential for dimerization exhibited by aluminum and boron catalysts.[15,16] In addition, many TMCCs are easy to handle on any scale. A systematic understanding of the influence of the metal center and ligands on the properties of a TMCC can be used to improve its performance as a catalyst.

1,10-Phenanthroline has been widely studied in solution.[17−21] Irving and co-workers measured binding constants of the complexed forms of Phen and derivatives of Phen in solution using spectrophotometric techniques. Although the thermodynamic information obtained from their studies is reliable, the measured binding constants are influenced by both the solvent and the counterions. The gas phase provides an ideal environment for examining the intrinsic binding in the absence of solvent effects and counterions. The ability to produce both coordinatively saturated and unsaturated complexes in the gas phase also allows the binding interactions to be examined as a function of the extent of ligation.

In this study, we characterize the structures and binding energies of divalent transition metal cation−Phen complexes. In particular, we elucidate the influence of the electronic structure of the transition metal cation on the geometric structure and strength of binding by systematically varying the metal cation from $Fe^{2+}(d^6)$ to $Co^{2+}(d^7)$ to $Ni^{2+}(d^8)$ to $Cu^{2+}(d^9)$ to $Zn^{2+}(d^{10})$. Previous work in our laboratory focused on the coordination behavior of singly charged transition metal cations with Phen ligands to examine how the electronic structure of

Received: February 18, 2013
Revised: April 6, 2013
Published: April 8, 2013

   dx.doi.org/10.1021/jp401711c | J. Phys. Chem. A 2013, 117, 4316−4330

the metal cation and chelation interactions influence the geometry and strength of binding.[22−25] In this work, studies of the analogous complexes in their +2 oxidation state allow the influence of the charge/oxidation state of the metal cation on the binding interactions to also be elucidated. The interactions between Phen and the five late first-row divalent transition metal cations are examined by measuring the kinetic energy dependence of their collision-induced dissociation (CID) behavior and performing complementary electronic structure theory calculations. Complexes with one to three Phen ligands are investigated theoretically, while experimental studies presented here are limited to the tris-complexes, $M^{2+}(Phen)_3$. The energy-resolved CID processes are analyzed using methods developed previously.[26] The analysis explicitly includes the effects of the internal and translational energy distributions of the reactants, multiple ion−neutral collisions, and their lifetimes for dissociation. We derive the third sequential bond dissociation energies (BDEs) of five $M^{2+}(Phen)_3$ complexes and compare these results to values obtained from density functional theory calculations performed here. Periodic trends in the structures and BDEs of these complexes are examined and compared to the analogous Phen complexes to the monovalent first-row transition metal cations, Co^+, Ni^+, Cu^+, and Zn^+, previously investigated.[22−25]

EXPERIMENTAL SECTION

Synthesis of 1,10-Phenanthroline Complexes. All chemicals were procured from commercial sources and used as received without further purification. The synthesis of $[M(Phen)_3](PF_6)_2$, where M = Fe, Co, Ni, Cu, and Zn, was carried out by adapting literature procedures[27,28] using $(NH_4)_2Fe(SO_4)_2$, $CoCl_2$, $Ni(NO_3)_2$, $Cu(NO_3)_2$, and $Zn(NO_3)_2$ salts, respectively. The $M^{2+}(Phen)_3$ complexes are obtained by reacting 3.0 equiv of the Phen ligand with 1.0 equiv of the metal salt. After 15 min of reflux, a methanolic solution of NH_4PF_6 is added to facilitate precipitation of the $[M(Phen)_3](PF_6)_2$ salt, which is isolated by filtration.

General Procedures. Cross sections for CID of five $M^{2+}(Phen)_3$ complexes with Xe, where M^{2+} = Fe^{2+}, Co^{2+}, Ni^{2+}, Cu^{2+}, and Zn^{2+}, are measured using a guided ion beam tandem mass spectrometer (GIBMS) that has been described previously.[29] The $M^{2+}(Phen)_3$ complexes are generated using an electrospray ionization (ESI) source that has been described in detail previously.[30] HPLC grade acetonitrile and deionized water were used to prepare solutions containing concentrations of ∼0.01−0.1 mM $[M(Phen)_3](PF_6)_2$ in a 1:1 (v/v) acetonitrile−water mixture. The ions emanating from the spray are desolvated, focused, and thermalized in a radio frequency (rf) ion funnel and hexapole ion guide collision cell interface. The thermalized ions emanating from the hexapole ion guide are extracted, accelerated, and focused into a magnetic sector momentum analyzer for mass analysis. Mass-selected ions are decelerated to a desired kinetic energy and focused into a rf octopole ion beam guide that traps the ions radially.[31,32] The octopole passes through a static gas cell containing Xe. The Xe pressure is kept low (∼0.025−0.20 mTorr) to ensure that multiple $M^{2+}(Phen)_3$−Xe collisions are improbable. Xenon is used in virtually all of our CID experiments because it is heavy and polarizable and therefore leads to more efficient kinetic to internal energy transfer in CID processes.[33,34] Products and undissociated $M^{2+}(Phen)_3$ complexes drift to the end of the octopole where they are focused into a quadrupole mass filter for mass analysis and detected using a secondary electron scintillation (Daly) detector and standard pulse counting techniques.

Data Handling. Ion intensities are converted to absolute cross sections using a Beer's law analysis as described previously.[35] Absolute uncertainties in the cross sections are derived largely from errors in the pressure measurements and uncertainty in the effective length of the interaction region and are estimated to be ±20%. Relative uncertainties are approximately ±5%.

Ion kinetic energies in the laboratory frame, E_{lab}, are converted to energies in the center-of-mass frame, E_{cm}, using the formula $E_{cm} = E_{lab}m/(m + M)$, where M and m are the masses of the $M^{2+}(Phen)_3$ and Xe reactants, respectively. Because the ions are doubly charged, the laboratory energies $E_{lab} = 2V_{lab}$, where V_{lab} is the applied voltage in the octopole region. All energies reported below are in the center-of-mass frame unless otherwise noted. The absolute zero and distribution of ion kinetic energies are determined using the octopole ion guide as a retarding potential analyzer as previously described.[35] The distribution of kinetic energies is nearly Gaussian with a full width at half-maximum (fwhm) between 0.2 and 0.4 eV (lab) for these experiments. The uncertainty in the absolute energy scale is ±0.10 eV (lab).

Because multiple ion−neutral collisions can influence the shape of CID cross sections, and the threshold regions are most sensitive to these effects, each CID cross section was measured twice at four nominal pressures of Xe, 0.025, 0.05, 0.10, and 0.20 mTorr. The measured CID cross sections exhibit a quadratic dependence on pressure in the threshold region. Data free from pressure effects are obtained by extrapolating to zero pressure of the neutral Xe reactant to ensure that cross sections subjected to thermochemical analysis are the results of single bimolecular encounters as previously described.[36]

Theoretical Calculations. To determine stable structures, molecular parameters needed for the thermochemical analysis of experimental data (i.e., vibrational frequencies and rotational constants) and energetics for the neutral Phen ligand and $M^{2+}(Phen)_x$ complexes, where M^{2+} = Fe^{2+}, Co^{2+}, Ni^{2+}, Cu^{2+}, and Zn^{2+} and x = 1−3, density functional theory (DFT) calculations were performed using the Gaussian 03[37] and Gaussian 09[38] suites of programs. The relative energies of all possible spin states of the $M^{2+}(Phen)_x$ complexes were carefully evaluated to determine the spin state of the ground-state species. In this work, the following spin states were examined: singlet, triplet, and quintet for $Fe^{2+}(Phen)_x$; doublet and quartet for $Co^{2+}(Phen)_x$; singlet and triplet for $Ni^{2+}(Phen)_x$; doublet for $Cu^{2+}(Phen)_x$; and singlet for $Zn^{2+}(Phen)_x$ complexes. Geometry optimizations and frequency analyses were performed at the B3LYP, BHandHLYP, and M06 levels of theory using the 6-31G* basis set. In all cases, the default methods were used such that for closed shell systems (having an even number of electrons divided into pairs of opposite spin) a spin-restricted model is used, while for open shell systems (possessing an unequal number of spin up and spin down electrons) a spin unrestricted model is employed. The B3LYP method has seen widespread use and has been shown to reliably predict energetics for most monovalent transition metal containing systems.[22−25] The BHandHLYP functional is also examined as its overall performance for treating the spin multiplicity of transition metal containing systems has recently been shown to be better than that of B3LYP.[39] The M06 functional has also been shown to be reasonably accurate and affordable for computations of transition metal systems.[40] The

dx.doi.org/10.1021/jp401711c | J. Phys. Chem. A 2013, 117, 4316−4330

computed vibrational frequencies were scaled by factors of 0.9804, 0.9472, and 0.9940 for the geometries determined using the B3LYP, BHandHLYP, and M06 functionals, respectively.[41−43] Vibrational frequencies and rotational constants of the structures optimized using the B3LYP functional were used in the modeling procedures. The B3LYP scaled vibrational frequencies and rotational constants for the ground-state structures of Phen and the $M^{2+}(Phen)_x$ complexes, where x = 1−3, as well as the quintet excited state of $Fe^{2+}(Phen)_3$ are listed in Tables S1 and S2 of the Supporting Information. Single-point energies were calculated at the B3LYP, BHandHLYP, and M06 levels of theory with a 6-311+G(2d,2p) basis set using the B3LYP/6-31G*, BHandHLYP/6-31G*, and M06/6-31G* optimized geometries, respectively. To obtain accurate energetics, zero-point energy (ZPE) and basis set superposition error (BSSE) corrections[44,45] were also included in the computed dissociation energies. The measured and calculated dipole moments and isotropic molecular polarizabilities of the neutral Phen ligand have been reported previously.[22,46]

Thermochemical Analysis. The threshold regions of the measured CID cross sections are modeled using an empirical threshold law, eq 1

$$\sigma(E) = \sigma_0 \sum_i g_i (E + E_i - E_0)^n / E \quad (1)$$

where σ_0 is an energy independent scaling factor, E is the relative translational energy of the reactants, E_0 is the threshold for reaction of the ground electronic and ro-vibrational state, and n is an adjustable parameter that is inversely correlated with the efficiency of kinetic to internal energy transfer.[47] The summation is over the ro-vibrational states of the reactant ions, i, where E_i are the excitation energies and g_i the populations of those states ($\sum g_i$ = 1). Because the $M^{2+}(Phen)_3$ complexes exhibit many low-frequency vibrational modes, the populations of excited vibrational modes are not negligible even at 298 K. Thus, the internal energy of the $M^{2+}(Phen)_3$ complex contributes significantly to the reaction threshold. The relative reactivity of all ro-vibrational states, as reflected by σ_0 and n, is assumed to be equivalent. The Beyer−Swinehart algorithm[48−50] is used to evaluate the density of the ro-vibrational states, and the relative populations, g_i, are calculated for a Maxwell−Boltzmann distribution at 298 K, the internal temperature of the $M^{2+}(Phen)_3$ complexes. The average internal energy of the ground-state conformations of the $M^{2+}(Phen)_3$ complexes and the quintet excited state of $Fe^{2+}(Phen)_3$ are included in the Supporting Information, Table S1. To account for inaccuracies in the computed frequencies, we have scaled the computed frequencies (prescaled by 0.9804) by ±10%. The corresponding change in the average vibrational energy is taken to be an estimate of one standard deviation of the uncertainty in the vibrational energy (Table S1).

An important consideration in the analysis of the $M^{2+}(Phen)_3$ CID thresholds is whether dissociation occurs within the ~10^{-4} s it takes for the complex to pass from the collision cell to the quadrupole mass filter. If the lifetime of the activated complex exceeds this time frame, the apparent thresholds are shifted to higher energies, resulting in a kinetic shift. For the $M^{2+}(Phen)_3$ complexes, with 195 vibrational modes over which the internal energy is randomized, this effect is significant. Therefore, the CID cross sections are analyzed by incorporating Rice−Ramsperger−Kassel−Marcus (RRKM) statistical theories into eq 1 as described in detail elsewhere.[26,51] In our analyses, the transition states (TSs) are assumed to be loose and product-like because the interactions between the $M^{2+}(Phen)_2$ complex and the departing Phen ligand are largely electrostatic. Therefore, the best model to describe such electrostatically bound complexes is a loose phase space limit (PSL) TS as described in detail elsewhere.[26] The parameters appropriate for the PSL TS are the frequencies and rotational constants of the $M^{2+}(Phen)_2$ and Phen CID products, which are taken from the B3LYP/6-31G* density functional theory (DFT) calculations performed here. The molecular parameters for the energized molecule are simply those of the reactant $M^{2+}(Phen)_3$ cation. The synthetic procedures employed for generation of the $M^{2+}(Phen)_3$ reactant cations should produce a racemic mixture of the Δ and Λ enantiomers. Because the relative computed stabilities of these enantiomers are within 1 kJ/mol for all five $M^{2+}(Phen)_3$ complexes, the measured BDEs describe the binding energies for either enantiomer. The rotational constants and vibrational frequencies for the energized molecules and the PSL TSs leading to dissociation are given in the Supporting Information in Tables S1 and S2.

The model represented by eq 1 is expected to be appropriate for translationally driven reactions.[52] The model is convoluted with the kinetic energy distributions of both reactants, and a nonlinear least-squares analysis of the data is performed to determine optimized values for the parameters σ_0, E_0 or E_0(PSL), and n. The error associated with the measurement of E_0 and E_0(PSL) is estimated from the range of threshold values determined for different data sets, variations associated with uncertainties in the vibrational frequencies (±10% scaling), and the error in the absolute energy scale, ±0.10 eV (E_{lab}). For analyses that include the RRKM lifetime analysis, the uncertainties in the reported E_0(PSL) values also include the effects of increasing and decreasing the time assumed available for dissociation (~10^{-4} s) by a factor of 2. Equation 1 explicitly includes the internal energy of the ion, E_i. All energy available is treated statistically because the internal (rotational and vibrational) energy of the reactants is redistributed throughout the $M^{2+}(Phen)_3$ complex upon impact with Xe. The threshold energies for dissociation reactions determined by analysis with eq 1 are equated to 0 K BDEs, which should be valid for the simple noncovalent bond cleavage reactions examined here.[53]

RESULTS

Cross Sections for Collision-Induced Dissociation. Experimental cross sections were obtained for the interaction of Xe with five $M^{2+}(Phen)_3$ complexes, where M^{2+} = Fe^{2+}, Co^{2+}, Ni^{2+}, Cu^{2+}, and Zn^{2+}. Figure 1 shows representative data for the $Cu^{2+}(Phen)_3$ and $Zn^{2+}(Phen)_3$ complexes. The other $M^{2+}(Phen)_3$ complexes exhibit similar behavior and are shown in the Supporting Information as Figure S1. For all five $M^{2+}(Phen)_3$ complexes, simple CID resulting in loss of an intact Phen ligand, reactions 2, is observed as the dominant dissociation pathway over the entire range of collision energies examined, typically 0 to >11 eV.

$$M^{2+}(Phen)_x + Xe \rightarrow M^{2+}(Phen)_{x-1} + Phen + Xe \quad (2)$$

The apparent threshold for the $M^{2+}(Phen)_2$ CID product shifts to lower energies from Fe^{2+} to Co^{2+}, increases for Ni^{2+}, but then decreases again from Ni^{2+} to Cu^{2+} to Zn^{2+} as the d electron occupation of the metal cation increases from d^6 to d^{10} across this series. The magnitudes of the CID cross sections

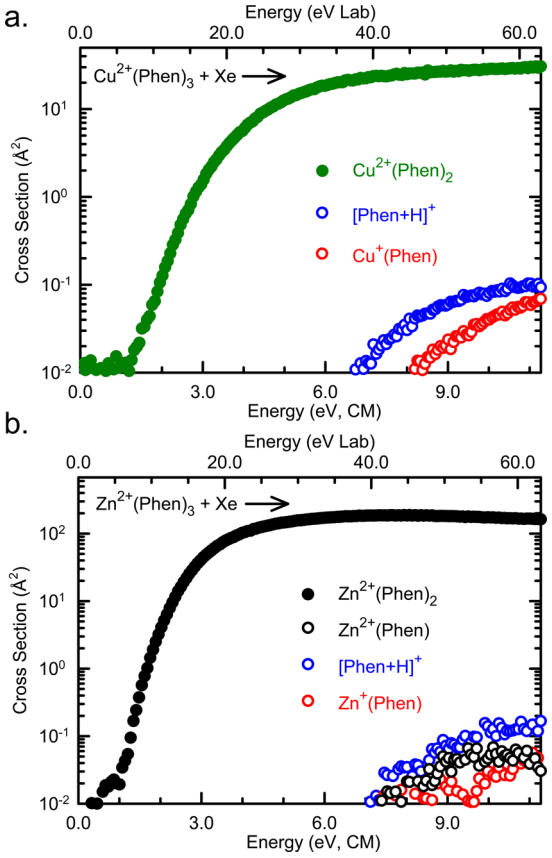

Figure 1. Cross sections for collision-induced dissociation of the $Cu^{2+}(Phen)_3$ and $Zn^{2+}(Phen)_3$ complexes, parts a and b, respectively, with Xe as a function of kinetic energy in the center-of-mass frame (lower *x*-axis) and laboratory frame (upper *x*-axis). Data are shown for a Xe pressure of ~0.2 mTorr.

generally follow the reverse trend. Sequential dissociation of the $M^{2+}(Phen)_2$ primary CID product is observed at elevated energies. Simple CID, reactions 2, resulting in the loss of a second Phen ligand is observed as a very minor sequential dissociation pathway only for the $Fe^{2+}(Phen)_3$ and $Zn^{2+}(Phen)_3$ complexes. Proton transfer Coulomb fission (PTCF), reactions 3, and electron transfer Coulomb fission (ETCF), reactions 4, are also observed as very minor sequential reaction pathways for all five of the $M^{2+}(Phen)_3$ complexes.

$$M^{2+}(Phen)_2 \rightarrow [M(Phen{-}H)]^+ + [Phen + H]^+ \quad (3)$$

$$M^{2+}(Phen)_2 \rightarrow M^+(Phen) + Phen^+ \quad (4)$$

Because the experiments were intentionally performed under low-resolution conditions to optimize sensitivity of the threshold determination, severe overlap of the $Phen^+$ and $[Phen+H]^+$ as well as the $[M(Phen{-}H)]^+$ and $M^+(Phen)$ sequential products is observed. Thus, only the species with the larger m/z of each pair were monitored, $[Phen+H]^+$ and $M^+(Phen)$. In all cases, PTCF is favored over ETCF as indicated by the larger cross section and lower apparent threshold of the $[Phen+H]^+$ products as compared to the $M^+(Phen)$ products. The simple CID, PTCF, and ETCF pathways resulting from the $M^{2+}(Phen)_2$ primary CID product will be investigated in detail in a follow-up to this study, where the CID of the $M^{2+}(Phen)_2$ complexes formed directly in the ESI process will be examined.

Threshold Analysis. The model of eq 1 was used to analyze the thresholds for CID reactions 2 of five $M^{2+}(Phen)_3$ complexes. The results of these analyses are provided in Table 1, and representative results for the $Cu^{2+}(Phen)_3$ and $Zn^{2+}(Phen)_3$ complexes are shown in Figure 2. The analyses for the other $M^{2+}(Phen)_3$ complexes are shown in the Supporting Information, Figure S2. In all cases, even after zero-pressure extrapolation, small low-energy features were observed in the CID cross sections suggesting that a small population (~3−4%) of vibrationally or electronically excited ions are present. Therefore, the model of eq 1 was used to analyze both raw zero-pressure extrapolated data and data obtained after subtraction of the low-energy feature. The low-energy feature can be reproduced nicely by shifting the threshold energy down by ~0.6−0.7 eV, retaining the same value of n as determined from fits to the dominant feature and reducing σ_0 by a factor of ~25−35 depending on the system. The model for the low-energy feature was then subtracted from the data and the remaining cross section reanalyzed to yield the analysis after subtraction of the low-energy feature. The modeling parameters for these analyses are given in Table 1. The difference in the thresholds for the two analyses are 0.23

Table 1. Modeling Parameters of Eq 1, Threshold Dissociation Energies at 0 K, and Entropies of Activation at 1000 K of $M^{2+}(Phen)_3$ Complexes[a]

M^{2+}	σ_0[b]	n[b]	E_0[c](eV)	E_0(PSL)[b](eV)	kinetic shift (eV)	$\Delta S^{\ddagger}$(PSL)[b](J mol^{-1} K^{-1})
Fe^{2+}	35.6 (11.2)	2.1 (0.1)	4.84 (0.31)	2.36 (0.12)	2.48	154.4 (4.3)
	72.4 (24.4)	*1.8 (0.2)*	*5.72 (0.30)*	*2.54 (0.13)*	*3.18*	*154.1 (4.3)*
	47.3 (11.0)	**2.0 (0.1)**	**5.03 (0.25)**	**2.11 (0.11)**	**2.92**	**90.8 (4.4)**
	103.5 (42.9)	***1.6 (0.2)***	***5.62 (0.28)***	***2.26 (0.12)***	***3.36***	***90.5 (4.4)***
Co^{2+}	59.5 (11.1)	1.9 (0.1)	4.48 (0.11)	2.00 (0.08)	2.48	94.0 (4.4)
	174.4 (12.2)	*1.3 (0.1)*	*5.36 (0.11)*	*2.23 (0.11)*	*3.13*	*93.5 (4.4)*
Ni^{2+}	53.8 (3.0)	1.9 (0.1)	4.96 (0.10)	2.14 (0.09)	2.82	98.4 (4.4)
	108.4 (8.1)	*1.5 (0.1)*	*5.52 (0.10)*	*2.28 (0.10)*	*3.24*	*98.1 (4.4)*
Cu^{2+}	30.4 (4.3)	2.3 (0.1)	3.02 (0.12)	1.50 (0.06)	1.52	67.3 (4.4)
	166.6 (25.5)	*1.2 (0.1)*	*3.99 (0.12)*	*1.81 (0.08)*	*2.18*	*66.5 (4.4)*
Zn^{2+}	54.9 (19.8)	2.0 (0.2)	3.17 (0.29)	1.58 (0.10)	1.59	77.6 (4.4)
	280.6 (88.8)	*1.0 (0.2)*	*4.34 (0.25)*	*1.95 (0.11)*	*2.39*	*76.7 (4.4)*

[a]Uncertainties are listed in parentheses. Analyses of raw zero-pressure extrapolated data are shown in standard font, while analyses of zero-pressure extrapolated data after subtraction of the low-energy feature are shown in italicized font. Analyses of the singlet state of the $Fe^{2+}(Phen)_3$ complex are shown in standard font, while those of the quintet state are shown in boldface. [b]Average values for loose PSL transition state. [c]No RRKM analysis.

dx.doi.org/10.1021/jp401711c | J. Phys. Chem. A 2013, 117, 4316−4330

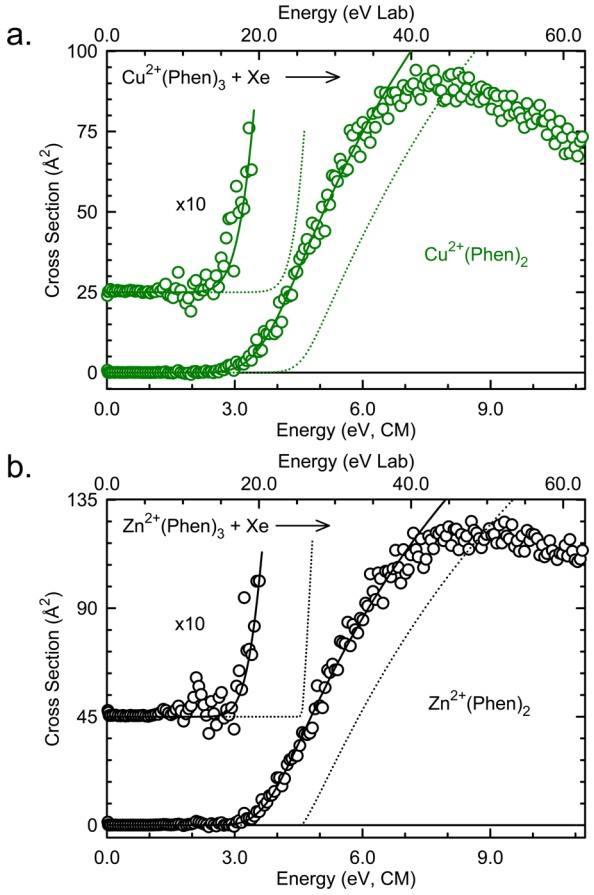

Figure 2. Zero-pressure-extrapolated cross sections for collision-induced dissociation of the $Cu^{2+}(Phen)_3$ and $Zn^{2+}(Phen)_3$ complexes, parts a and b, respectively, with Xe in the threshold region as a function of kinetic energy in the center-of-mass frame (lower *x*-axis) and laboratory frame (upper *x*-axis). Solid lines show the best fits to the data using eq 1 convoluted over the kinetic and internal energy distributions of the reactants. Dotted lines show the model cross sections in the absence of experimental kinetic energy broadening for reactants with an internal energy corresponding to 0 K.

eV for the complex to Co^{2+}, 0.14 eV for Ni^{2+}, 0.31 eV for Cu^{2+}, 0.37 eV for Zn^{2+}, 0.18 eV for the singlet ground state of $Fe^{2+}(Phen)_3$, and 0.15 eV for the quintet excited state of $Fe^{2+}(Phen)_3$. Figures 2 and S2 show the analysis after subtraction of the low-energy feature. As can be seen in the figures, the cross sections are reproduced by eq 1 over a large range of energies (>6 eV) and over 4 orders of magnitude. Previous work has shown that this model provides the most accurate assessment of the kinetic shifts for simple CID processes of electrostatically bound metal-ligand complexes.[22−24] Table 1 also includes the kinetic shifts observed from the difference in thresholds obtained with and without the inclusion of lifetime effects. The Fe^{2+}, Co^{2+}, and Ni^{2+} complexes exhibit similar kinetic shifts, which are significantly larger than those of the Cu^{2+} and Zn^{2+} complexes. Similarly, the binding in the Fe^{2+}, Co^{2+}, and Ni^{2+} complexes is stronger than in the Cu^{2+} and Zn^{2+} complexes. Because the total number of vibrations, 195, and heavy atoms, 43, and hence the number of low-frequency vibrations remains the same for all five $M^{2+}(Phen)_3$ complexes, the kinetic shifts should directly correlate with the density of states at threshold, which depends on the measured BDE, consistent with the results determined here. The large number of modes available to the $M^{2+}(Phen)_3$ complexes over which the internal energy can be randomized also results in relatively large *n* values, ~1.7 ± 0.1 for these systems.

The entropy of activation, $\Delta S^{\ddagger}$, describes the looseness of the TS and reflects the size and complexity of the system. It is largely determined by the molecular parameters used to model the energized molecule and the TS, but also depends on the threshold energy. Listed in Table 1, $\Delta S^{\ddagger}$(PSL) values at 1000 K vary between 66.5 and 154.4 J mol^{-1} K^{-1} and are directly correlated with the measured BDEs for these complexes. The relatively large entropies of activation determined for these systems are the result of the weak noncovalent binding of the third Phen ligand and conformational relaxation of the $M^{2+}(Phen)_2$ product resulting from the reduction in steric crowding upon dissociation.

Theoretical Results. Ground-state structures of the $M^{2+}(Phen)_x$ complexes, where M^{2+} = Fe^{2+}, Co^{2+}, Ni^{2+}, Cu^{2+}, and Zn^{2+} and *x* = 1−3, were calculated using the Gaussian 03[37] and Gaussian 09[38] suites of programs as described in the Theoretical Calculations section. The ground electronic spin states of the $M^{2+}(Phen)_x$ complexes to Co^{2+}, Ni^{2+}, Cu^{2+}, and Zn^{2+} were found to be quartet, triplet, doublet, and singlet, respectively, for all values of *x* = 1−3. For the $Fe^{2+}(Phen)$ and $Fe^{2+}(Phen)_2$ complexes, the ground electronic spin states were found to be quintet. The ground-state spin multiplicity of the $Fe^{2+}(Phen)_3$ complex was predicted to be low-spin singlet when the B3LYP functional was employed, whereas BHandHLYP and M06 predict the ground state to be high-spin quintet. Relative energies of the $M^{2+}(Phen)_x$ complexes, where *x* = 1−3, computed for the various possible spin states of each metal cation are summarized in Table S3.

The sequential BDEs calculated for all five of the $M^{2+}(Phen)_x$ complexes determined at the B3LYP/6-311+G(2d,2p)//B3LYP/6-31G*, BHandHLYP/6-311+G(2d,2p)//BHandHLYP/6-31G*, and M06/6-311+G(2d,2p)//M06/6-31G* levels of theory including independent ZPE and BSSE corrections are listed in Table 2. The B3LYP functional was found to deliver results that are most consistent with values measured for the third sequential binding energies. Therefore, except as noted, the following discussion is based on the B3LYP results. The B3LYP/6-31G* optimized geometries of the $M^{2+}(Phen)_x$ complexes are shown in Figure 3 and Figure S4 of the Supporting Information. Relevant structural details of the optimized structures for each of these species are listed in Table 3 and Table S4 of the Supporting Information. In the ground-state structures, the metal cation binds to the Phen ligand(s) through the lone pairs of both nitrogen atoms, in agreement with previous results obtained for the analogous singly charged complexes.[22−25] Theoretical details regarding the geometry, dipole moment, and isotropic molecular polarizability of the Phen ligand have been reported previously.[22] The calculated dipole moment and isotropic molecular polarizability of Phen are 3.31 D and 23.78 Å^3, respectively, relatively large values as a result of the extended π network of this planar and rigid molecule.

$M^{2+}(Phen)_x$ Complexes, M^{2+} = Fe^{2+}, Co^{2+}, Ni^{2+}, and Zn^{2+}. The B3LYP/6-31G* ground-state structures of the $M^{2+}(Phen)_x$ complexes where M^{2+} = Fe^{2+}, Co^{2+}, Ni^{2+}, and Zn^{2+} are shown in Figure 3 and Figure S4 of the Supporting Information. In the monocomplexes, $M^{2+}(Phen)$, the metal cation binds to the lone pairs of both nitrogen atoms of the Phen ligand, resulting in a bent geometry of the N donor atoms around the metal cation as a result of the structural rigidity of the Phen ligand. The two M^{2+}−N bond lengths are equal and

dx.doi.org/10.1021/jp401711c | J. Phys. Chem. A 2013, 117, 4316−4330

Table 2. Measured and Calculated Sequential and Total Enthalpies of Binding of $M^{2+}(Phen)_x$ Complexes at 0 K in kJ/mol

		theory								
		B3LYP[b]			BHandHLYP[c]			M06[d]		
complex	TCID[a]	D_0	$D_{0,BSSE}$[e]	total[e]	D_0	$D_{0,BSSE}$[e]	total[e]	D_0	$D_{0,BSSE}$[e]	total[e]
$Fe^{2+}(Phen)$	–	1021.2	1018.3	1018.3	939.6	936.4	936.4	991.7	988.3	988.3
$Fe^{2+}(Phen)_2$	–	515.6	511.8	1530.1	547.0	543.0	1479.4	572.8	567.9	1556.2
$Fe^{2+}(Phen)_3$	236.5 (17.0)	223.0	215.0	1745.1	234.1	226.5	1705.9	275.8	265.4	1821.6
$Fe^{2+}(Phen)_3$	**210.7 (11.1)**	**220.5**	**212.5**	**1742.6**	**331.2**	**323.6**	**1803.0**	**314.2**	**303.8**	**1860.0**
$Co^{2+}(Phen)$	–	1084.4	1080.9	1080.9	1015.0	1011.6	1011.6	1085.4	1081.3	1081.3
$Co^{2+}(Phen)_2$	–	549.8	545.2	1626.1	557.7	553.3	1564.9	573.1	567.0	1648.3
$Co^{2+}(Phen)_3$	203.8 (12.3)	200.1	193.6	1819.7	223.3	216.8	1781.7	272.3	264.2	1912.5
$Ni^{2+}(Phen)$	–	1157.9	1154.4	1154.4	1079.0	1076.1	1076.1	1202.0	1197.2	1197.2
$Ni^{2+}(Phen)_2$	–	542.1	537.5	1691.9	523.7	519.1	1595.2	556.4	551.2	1748.4
$Ni^{2+}(Phen)_3$	213.2 (12.8)	240.3	233.2	1925.1	287.0	280.1	1875.3	312.6	303.7	2052.1
$Cu^{2+}(Phen)$	–	1262.8	1259.1	1259.1	1154.3	1151.3	1151.3	1256.4	1252.6	1252.6
$Cu^{2+}(Phen)_2$	–	518.9	514.0	1773.1	546.3	540.9	1692.2	544.1	538.4	1791.0
$Cu^{2+}(Phen)_3$	159.6 (9.9)	156.0	149.1	1922.2	174.5	167.5	1859.7	211.6	203.2	1994.2
$Zn^{2+}(Phen)$	–	1126.3	1123.3	1123.3	1084.2	1081.2	1081.2	1114.2	1111.1	1111.1
$Zn^{2+}(Phen)_2$	–	544.7	540.4	1663.7	555.7	551.4	1632.6	561.1	556.0	1667.1
$Zn^{2+}(Phen)_3$	170.1 (14.3)	171.0	163.9	1827.6	192.2	185.1	1817.7	233.4	225.4	1892.5
AEU/MAD[f]	13.3 (2.6)		13.7 (6.7)			22.3 (25.1)			56.2 (22.3)	
AEU/MAD[g]	**12.1 (1.9)**		**9.7 (6.7)**			**43.2 (45.7)**			**68.6 (22.1)**	

[a]Average values from fits to raw data and data after subtraction of the low-energy feature, Table 1. Average values for the singlet state of $Fe^{2+}(Phen)_3$ complex are shown in standard font, while those of the quintet state of $Fe^{2+}(Phen)_3$ are shown in boldface. [b]Calculated at the B3LYP/6-311+G(2d,2p)//B3LYP/6-31G* level of theory including ZPE corrections with frequencies scaled by 0.9804. [c]Calculated at the BHandHLYP/6-311+G(2d,2p)//BHandHLYP/6-31G* level of theory including ZPE corrections with frequencies scaled by 0.9472. [d]Calculated at the M06/6-311+G(2d,2p)//M06/6-31G* level of theory including ZPE corrections with frequencies scaled by 0.9940. [e]Also includes BSSE corrections. [f]AEU/MAD values using the singlet state of $Fe^{2+}(Phen)_3$ in the analysis. [g]AEU/MAD values using the quintet state of $Fe^{2+}(Phen)_3$ in the analysis.

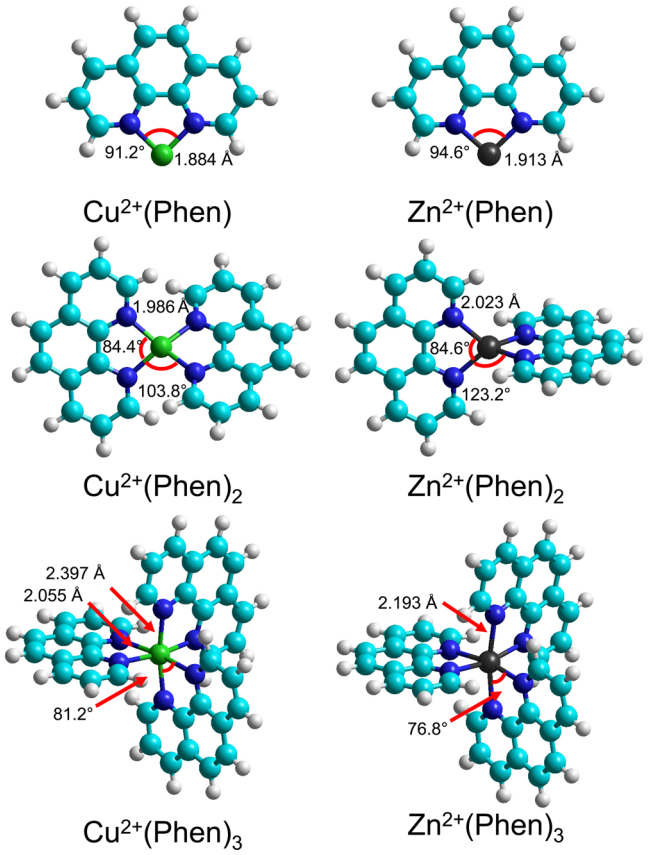

Figure 3. B3LYP/6-31G* optimized geometries of $Cu^{2+}(Phen)_x$ and $Zn^{2+}(Phen)_x$ complexes, where x = 1–3.

decrease from Fe^{2+} (1.967 Å) to Co^{2+} (1.934 Å) to Ni^{2+} (1.892 Å) and then slightly increase again for Zn^{2+} (1.913 Å). The decrease in the bond lengths from Fe^{2+} to Co^{2+} to Ni^{2+} closely matches the decrease in the radii of these metal cations: 0.76, 0.74, and 0.73 Å, respectively. Zn^{2+} deviates from this simple trend as its radius, 0.72 Å, is the smallest.[54,55] The $\angle NM^{2+}N$ bond angles decrease from Fe^{2+} (90.9°) to Co^{2+} (89.9°), and then increase from Ni^{2+}(91.6°) to Zn^{2+}(94.6°), nearly parallel in behavior to the variations in the M^{2+}–N bond lengths. The ∠NCCN dihedral angles are 0.0° for all of the monocomplexes as found for the free Phen ligand.

In the bis-complexes, the metal cation coordinates to all four nitrogen atoms of the two Phen ligands in a distorted tetrahedral coordination geometry. The structural rigidity of the Phen ligands prevents the ideal tetrahedral coordination geometry from being achieved. The two Phen ligands are nearly perpendicular to one another, with an $\angle NM^{2+}NC$ dihedral angle of ~81.2°. The four M^{2+}–N bond lengths are equal and decrease from Fe^{2+} (2.062 Å) to Co^{2+} (2.024 Å) to Ni^{2+} (2.003 Å), and then slightly increase for Zn^{2+} (2.023 Å), parallel to that found for the monocomplexes. The intraligand $\angle NM^{2+}N$ bond angles vary between 83.0° and 84.6°, while the interligand $\angle NM^{2+}N$ bond angles vary between 123.2° and 124.1°. The ∠NCCN dihedral angles in all of the bis-complexes are ~0.0° as found for the free Phen ligand and $M^{2+}(Phen)$ complexes.

In the tris-complexes, all six nitrogen atoms of the three Phen ligands are coordinated to the metal cation in a distorted octahedral arrangement. The six M^{2+}–N bond lengths are equal and decrease from Fe^{2+} (2.204 Å) to Co^{2+} (2.163 Å) to Ni^{2+} (2.117 Å), and then slightly increase for Zn^{2+} (2.193 Å) when comparing the quintet state of $Fe^{2+}(Phen)_3$, again parallel to that found for the mono- and bis-complexes. However, the spin

dx.doi.org/10.1021/jp401711c | J. Phys. Chem. A 2013, 117, 4316–4330

Table 3. Geometrical Parameters of the B3LYP/6-31G* Ground-State Structures of the Neutral Phen Ligand and $M^{2+}(Phen)_x$ Complexes[a]

complex	M^{2+}–N	∠NCCN	∠NM^{2+}NC	∠NM^{2+}N[b]	∠NM^{2+}N[c]
Phen	–	0.0	–	–	–
$Fe^{2+}(Phen)$	1.967	0.0	–	90.9	–
$Fe^{2+}(Phen)_2$	2.062	0.0	81.1	83.0	124.1
$Fe^{2+}(Phen)_3$	2.006	1.3	60.4	82.1	89.1 (3), 94.5 (6), 175.3 (3)
$Fe^{2+}(Phen)_3$	**2.204**	**1.3 (2), 1.8**	**57.0**	**76.4**	**91.4, 94.2 (4), 96.3 (4), 167.1, 169.6 (2)**
$Co^{2+}(Phen)$	1.934	0.0	–	89.9	–
$Co^{2+}(Phen)_2$	2.024	0.0	81.2	84.2	123.4
$Co^{2+}(Phen)_3$	2.163	1.2	61.1	77.6	89.5 (3), 96.7 (6), 172.1 (3)
$Ni^{2+}(Phen)$	1.892	0.0	–	91.6	–
$Ni^{2+}(Phen)_2$	2.003	0.0	82.1	83.3	124.0
$Ni^{2+}(Phen)_3$	2.117	1.5 (2), 1.3	59.3	79.3	90.7 (3), 95.2 (6), 172.3 (3)
$Cu^{2+}(Phen)$	1.884	0.0	–	91.2	–
$Cu^{2+}(Phen)_2$	1.986	0.9	49.0	84.4	103.8 (2), 149.2 (2)
$Cu^{2+}(Phen)_3$	2.055 (4), 2.397(2)	2.3 (2), 0.4	56.9	75.8 (2), 81.2	91.3 (3), 94.3 (4), 99.1 (2), 170.4 (3)
$Zn^{2+}(Phen)$	1.913	0.0	–	94.6	–
$Zn^{2+}(Phen)_2$	2.023	0.0	81.1	84.6	123.2
$Zn^{2+}(Phen)_3$	2.193	1.7	56.9	76.8	94.8 (9), 168.4 (3)

[a]Average values are given for similar bond distances or angles; degeneracies are listed in parentheses for values that differ sufficiently such that more than one value is needed to describe the bond angle or bond distance. Geometrical parameters for the singlet ground-state of $Fe^{2+}(Phen)_3$ are shown in standard font, while those for quintet excited-state are shown in boldface. All bond angles (∠) are given in degrees (°) and M^{2+}–N bond lengths in angstroms (Å). [b]Intraligand angles. [c]Interligand angles.

change to singlet results in shorter Fe^{2+}–N bond lengths of 2.006 Å in the ground-state $Fe^{2+}(Phen)_3$ complex. The intraligand ∠NM^{2+}N bond angles are ~78.0°, significantly smaller than the octahedral value of 90.0°. The interligand ∠NM^{2+}N bond angles for the N atoms cis to each other are ~95.0°, whereas for the trans N atoms, these angles are ~169.0°. These deviations from perfect octahedral coordination are again the result of the structural rigidity of the Phen ligands. The individual Phen ligands are nearly planar, with average ∠NCCN dihedral angles of 1.3° for two of the Phen ligands and 1.8° for the third Phen ligand. The dihedral angle between any two Phen ligands varies between 57.1° and 60.6°. In all cases, the M^{2+}–N bond lengths increase with increasing ligation as shown in Figure 3 and Figures S3 and S4 of the Supporting Information, as a result of the decreasing electrostatic attraction between the metal cation and the Phen ligands and increasing ligand–ligand repulsive interactions. Only $Fe^{2+}(Phen)_3$ deviates from these trends as a result of the spin crossover from quintet to singlet upon binding of the third ligand. As the bond lengths increase, the intraligand ∠NM^{2+}N bond angles decrease.

$Cu^{2+}(Phen)_x$ Complexes. As found for the $M^{2+}(Phen)_x$ complexes to Fe^{2+}, Co^{2+}, Ni^{2+}, and Zn^{2+}, the Phen ligands bind to Cu^{2+} via the lone pairs of both nitrogen atoms, leading to similar bent, distorted tetrahedral, and distorted octahedral geometries for the mono-, bis-, and tris-complexes to Cu^{2+}, respectively. In the $Cu^{2+}(Phen)$ complex, the Cu^{2+}–N bond distances are 1.884 Å and the ∠NCu^{2+}N bond angle is 91.2°. In the $Cu^{2+}(Phen)_2$ complex, the Cu^{2+}–N bond lengths increase to 1.986 Å. The bond angles between Cu^{2+} and the N atoms differ slightly, with intraligand ∠NCu^{2+}N angles of 84.4° and interligand ∠NCu^{2+}N bond angles of 103.8° and 149.2°. The individual Phen ligands are almost planar with average ∠NCCN dihedral angles of 0.9°. The planes of the two Phen ligands are twisted relative to each other with ∠NM^{2+}NC dihedral angles of 49.0°. In contrast, the other $M^{2+}(Phen)_2$ complexes exhibit much larger ∠NM^{2+}NC dihedral angles of 81.2°. The tris-complex is tetragonally elongated such that the Cu^{2+}–N bond distances of the four equatorial nitrogen atoms are 2.055 Å, while the Cu^{2+}–N bond distances are 2.397 Å for the axial nitrogen atoms. The relevant intra- and interligand ∠NCu^{2+}N bond angles that define the distorted octahedral geometry (and their degeneracies) are 75.8°(2) and 81.2°, and 91.3°(3), 94.3°(4), 99.1°(2), and 170.4°(3), respectively. The distortions from the idealized tetrahedral and octahedral geometries of the bis- and tris-complexes are more severe for the $Cu^{2+}(Phen)_x$ complexes than for the other metal cations. Similar to the other $M^{2+}(Phen)_x$ complexes, as the number of Phen ligands increases, the Cu^{2+}–N bond lengths increase due to decreasing electrostatic attractions and increasing ligand–ligand repulsive interactions as shown in Figure 3 and Figure S3 of the Supporting Information. As the Cu^{2+}–N bond lengths increase, the intraligand ∠NCu^{2+}N bond angles decrease, while the trans interligand bond angles increase to minimize ligand repulsive interactions.

Conversion from 0 to 298 K. Conversion of the measured and calculated BDEs determined here at 0 K to 298 K bond enthalpies and free energies was performed to allow comparison to commonly employed experimental conditions. The enthalpy and entropy conversions are calculated using standard formulas (assuming harmonic oscillator and rigid rotor models) and the vibrational and rotational constants determined for the B3LYP/6-31G* optimized geometries, which are given in Tables S1 and S2 of the Supporting Information. Table 4 lists 0 and 298 K enthalpies, free energies, and enthalpic and entropic corrections for all systems experimentally and theoretically determined. Uncertainties in these values are determined by ±10% variations in the vibrational frequencies and additionally by scaling the metal–ligand frequencies up and down by a factor of 2.

DISCUSSION

Metal–Ligand Bonding Interactions of the $M^{2+}(Phen)_3$ Complexes. The metal–ligand bonding interactions in the

dx.doi.org/10.1021/jp401711c | J. Phys. Chem. A 2013, 117, 4316–4330

Table 4. Enthalpies and Free Energies of Binding of $M^{2+}(Phen)_x$ Complexes at 0 and 298 K in kJ/mol[a]

complex	ΔH_0	ΔH_0[b]	$\Delta H_{298} - \Delta H_0$[b]	ΔH_{298}	ΔH_{298}[b]	$T\Delta S_{298}$[b]	ΔG_{298}	ΔG_{298}[b]
$Fe^{2+}(Phen)$	–	1018.3	2.4 (0.3)	–	1020.7	33.5 (0.5)	–	987.2
$Fe^{2+}(Phen)_2$	–	511.8	−1.3 (0.9)	–	510.5	51.6 (1.6)	–	458.9
$Fe^{2+}(Phen)_3$	236.5 (17.0)	215.0	−2.3 (0.7)	234.2 (17.0)	212.7	55.2 (1.4)	179.0 (17.1)	157.5
$Fe^{2+}(Phen)_3$	**210.7 (11.1)**	**212.5**	**−2.3 (0.7)**	**208.4 (11.1)**	**210.2**	**55.2 (1.4)**	**153.2 (11.2)**	**155.0**
$Co^{2+}(Phen)$	–	1080.9	2.6 (0.3)	–	1083.5	36.3 (0.4)	–	1047.2
$Co^{2+}(Phen)_2$	–	545.2	−0.2 (0.9)	–	545.0	54.7 (1.5)	–	490.3
$Co^{2+}(Phen)_3$	203.8 (12.3)	193.6	−2.4 (0.6)	201.4 (12.3)	191.2	56.1 (1.4)	145.3 (12.4)	135.1
$Ni^{2+}(Phen)$	–	1154.4	2.6 (0.3)	–	1157.0	36.5 (0.4)	–	1120.5
$Ni^{2+}(Phen)_2$	–	537.5	−0.4 (0.9)	–	537.1	53.7 (1.5)	–	483.4
$Ni^{2+}(Phen)_3$	213.2 (12.8)	233.2	−2.2 (0.7)	211.0 (12.8)	231.0	57.3 (1.4)	153.7 (12.9)	173.7
$Cu^{2+}(Phen)$	–	1259.1	1.6 (0.3)	–	1260.7	33.4 (0.5)	–	1227.3
$Cu^{2+}(Phen)_2$	–	514.0	0.5 (0.8)	–	514.5	56.9 (1.4)	–	457.6
$Cu^{2+}(Phen)_3$	159.6 (9.9)	149.1	−3.6 (0.9)	156.0 (9.9)	145.5	50.2 (1.8)	105.8 (10.1)	95.3
$Zn^{2+}(Phen)$	–	1123.3	2.6 (0.3)	–	1125.9	36.6 (0.4)	–	1089.3
$Zn^{2+}(Phen)_2$	–	540.4	−1.0 (0.9)	–	539.4	52.8 (1.6)	–	486.6
$Zn^{2+}(Phen)_3$	170.1 (14.3)	163.9	−3.4 (0.7)	166.5 (14.3)	160.5	52.1 (1.6)	114.4 (14.4)	108.4

[a]Uncertainties are listed in parentheses. Values of singlet ground-state $Fe^{2+}(Phen)_3$ are shown in standard font, while those of quintet excited-state $Fe^{2+}(Phen)_3$ are shown in boldface. [b]Values from calculations at the B3LYP/6-311+G(2d,2p) level of theory using B3LYP/6-31G* optimized geometries with frequencies scaled by 0.9804.

$M^{2+}(Phen)_3$ complexes involve the metal 3d orbitals, the σ lone pairs on the N atoms, and the delocalized π systems of the Phen ligands. The principal bonding mechanisms feature electron donation from the lone pairs of the N atoms to the metal with a synergic back-bonding contribution from the occupied metal d_π orbitals to vacant π^* orbitals of the Phen ligands. The metal 3d orbitals, transforming as d_π (d_{xy}, d_{xz}, d_{yz}) and d_{σ^*} (d_{z^2} and $d_{x^2-y^2}$) orbitals are split through interaction with the Phen ligand orbitals of similar symmetry. The magnitude of the energy difference between the d_π and d_{σ^*} set depends on the nature and number of the ligands bound to the metal center. When the ligand field splitting is small the electrons form a high-spin complex, where all of the unpaired spins are aligned as prescribed for the free metal cation by Hund's rule, to minimize electron−electron repulsion. When the ligand field splitting becomes large enough that the energy gained by dropping from the d_{σ^*} to the d_π level is sufficient to overcome the electron pairing energy, a low-spin complex results. Therefore, the ground-state spin of the $M^{2+}(Phen)_3$ complexes is determined by a balance between Hund's rule of maximum multiplicity, which favors high-spin states, and metal−ligand bonding, which favors low-spin states. On this basis the principal bonding interactions that occur between the metal 3d orbitals and the ligand π orbitals find the ground electronic spin states of the $M^{2+}(Phen)_x$ complexes to Co^{2+}, Ni^{2+}, Cu^{2+}, and Zn^{2+} to be quartet, triplet, doublet, and singlet, respectively, when the B3LYP, BHandHLYP, and M06 functionals are employed. For the $Fe^{2+}(Phen)$ and $Fe^{2+}(Phen)_2$ complexes, the ground electronic spin states were found to be quintet. In contrast, the ground-state spin multiplicity of the $Fe^{2+}(Phen)_3$ complex was predicted to be low-spin singlet when the B3LYP functional was employed, whereas BHandHLYP and M06 predicted the ground state to be high-spin quintet. The tendency of different density functionals to predict different ground electronic spin states for the $Fe^{2+}(Phen)_3$ complex is consistent with other recent theoretical calculations of related iron-containing compounds with spin states that lie close in energy.[56,57]

Previous studies have shown that spin crossover or spin transitions are involved in most complexes involving the Fe^{2+} ion.[58] These studies show that for the Fe^{2+} d^6 configuration in an octahedral field, there is a value for the ligand field strength beyond which the ground state of the Fe^{2+} ion changes from a quintet to singlet state. Hence, a spin crossover or spin transition can be expected to be induced when the ligand field strength about the Fe^{2+} ion is in the vicinity of this critical value such that minor external perturbations can tip the scales in favor of one or the other for the ground states.[59,60] For example, studies of Fe^{2+} complexes using Mossbauer spectroscopy indicate that quintet−singlet transitions of ground-state Fe^{2+} are temperature dependent.[61−64] Other studies have shown that the ligand structure can influence the symmetry of the Fe^{2+} ion environment causing spin transition.[17−21] Extensive data exist establishing that nearly all six-coordinate Fe^{2+} complexes of the type $Fe^{2+}(Phen)_3$ have diamagnetic ground states.[65] In the current studies, the progressive addition of Phen ligands to the Fe^{2+} center effects spin pairing in the Fe^{2+} ion only on coordination of the third Phen ligand according to B3LYP results. This is a clear indication that the ligand structure is influencing the symmetry of the Fe^{2+} ion environment causing a spin transition. The quintet and singlet states of the $Fe^{2+}(Phen)_x$ complexes possess four and zero unpaired electrons, respectively. In the $Fe^{2+}(Phen)$ and $Fe^{2+}(Phen)_2$ ions, the degenerate 3d levels split into three lower d_π and two higher energy d_{σ^*} orbitals, but the electrons are not spin-paired as the energy separation is insufficient to overcome the necessary interelectron repulsions. Under the stronger field splitting provided by three Phen ligands, the six electrons become spin-paired, so that a diamagnetic $Fe^{2+}(Phen)_3$ complex results. That the BHandHLYP and M06 functionals suggest a paramagnetic $M^{2+}(Phen)_3$ complex is due to the functionals overstabilizing the quintet state by about 97.1 and 38.4 kJ/mol over the singlet state, respectively. The small difference in energy computed between the quintet and the singlet states of $Fe^{2+}(Phen)_3$, ~2.5 kJ/mol using the B3LYP functional, indicates that the two states may coexist at room temperature.

To establish which electronic spin states of the $Fe^{2+}(Phen)_3$ complex are accessed in the experiments, the TCID experimental data for the $Fe^{2+}(Phen)_3$ system is analyzed

dx.doi.org/10.1021/jp401711c | J. Phys. Chem. A 2013, 117, 4316−4330

twice, once assuming that the threshold arises from dissociation of the singlet ground state, and the other assuming that the threshold describes dissociation from the quintet excited state. The BDE extracted assuming that the precursor $Fe^{2+}(Phen)_3$ complex is in the singlet ground state is 236.5 ± 17.0 kJ/mol, whereas the value extracted assuming that the threshold is influenced by the presence of a reasonable population of the quintet excited state is 210.7 ± 11.1 kJ/mol, the latter corresponding to a diabatic BDE for this system. As compared to the B3LYP values calculated for dissociation from the singlet ground state and quintet excited states of $Fe^{2+}(Phen)_3$, 215.0 and 212.5 kJ/mol, respectively, these analyses suggest that quintet excited state is indeed accessed in the experiments and shifts the threshold to lower values. These results are indeed consistent with the B3LYP results that indicate that ~37% of the ions should exist in the quintet excited state, whereas ~63% of the ions would exist in the singlet ground state at room temperature. Thus, the threshold should be determined by the dissociation behavior of the quintet excited state as it provides the lowest energy pathway to dissociation. Hence, the computed B3LYP BDEs and the TCID experimental results for the $Fe^{2+}(Phen)_3$ complex suggest that the singlet ground state and the excited quintet state of Fe^{2+} are both accessed in the experiments and that the threshold energy we measure for the third sequential binding energy of $Fe^{2+}(Phen)_3$ is more likely the diabatic value.

Trends in the BDEs of the $M^{2+}(Phen)_3$ Complexes. The measured BDEs of the $M^{2+}(Phen)_3$ complexes, where M^{2+} = Fe^{2+}, Co^{2+}, Ni^{2+}, Cu^{2+}, and Zn^{2+}, are illustrated in Figure 4 and summarized in Table 2 along with the corresponding theoretical BDEs calculated at the B3LYP/6-311+G(2d,2p), BHandHLYP/6-311+G(2d,2p), and M06/6-311+G(2d,2p) levels of theory. The measured BDEs are reported as the average values obtained from threshold analyses of the raw zero-pressure extrapolated data and analyses after subtraction of the low-energy feature, Table 1. At first glance, the stability of $M^{2+}(Phen)_3$ complexes should be dominated by electrostatic interactions, the strength of binding depending on the ionic radii, second ionization energies of the metal, and the M^{2+}–N bond lengths. However, the nature of Phen ligands also contributes. The measured BDEs of the $M^{2+}(Phen)_3$ complexes follow the order $Cu^{2+} < Zn^{2+} < Co^{2+} < Fe^{2+} < Ni^{2+}$ as shown in Figure 4. The size of the metal cation decreases as the d orbital occupation increases: 0.76, 0.74, 0.73, 0.72, and 0.72 Å for Fe^{2+}, Co^{2+}, Ni^{2+}, Cu^{2+}, and Zn^{2+}, respectively. Roughly parallel to the trend is the ionic radii of the metal cations; the M^{2+}–N bond lengths decrease from Fe^{2+} (2.204 Å) to Co^{2+} (2.163 Å) to Ni^{2+} (2.117 Å), and then increase for Zn^{2+} (2.193 Å) when comparing the quintet states. However, the spin change that the $Fe^{2+}(Phen)_3$ complex undergoes enables the ligands to approach the metal ion more closely resulting in a decrease in the M^{2+}–N bond lengths to 2.006 Å for $Fe^{2+}(Phen)_3$ in its singlet ground state. The structural variation observed in the $Cu^{2+}(Phen)_3$ complex resulting in two different Cu^{2+}–N bond lengths (2.055 and 2.397 Å) as compared to the $M^{2+}(Phen)_3$ complexes to Fe^{2+}, Co^{2+}, Ni^{2+}, and Zn^{2+} is due to Jahn–Teller effects by which the $Cu^{2+}(Phen)_3$ complex shows pronounced distortions leading to much weaker binding of the third Phen ligand. Although the difference in size between the metal cations is not that significant, the effective nuclear charge increases across the period, and therefore the binding interactions between the Phen ligands and M^{2+} cation is expected to increase across the period from Fe^{2+} to Zn^{2+}. The steric interactions between the bulky Phen ligands also lead to a lower binding energy, but this effect should be approximately independent of the identity of the metal cation. The weak BDEs of the $M^{2+}(Phen)_3$ complexes also confirm that the binding is noncovalent in nature. This is supported by the fact that in all the $M^{2+}(Phen)_3$ complexes, the most prominent fragmentation channel is the loss of an intact Phen ligand. The energy required to break a typical C–C covalent bond is >400 kJ/mol,[66] which is much greater than the BDEs of the $M^{2+}(Phen)_3$ complexes determined here, which are <240 kJ/mol for all five metal cations.

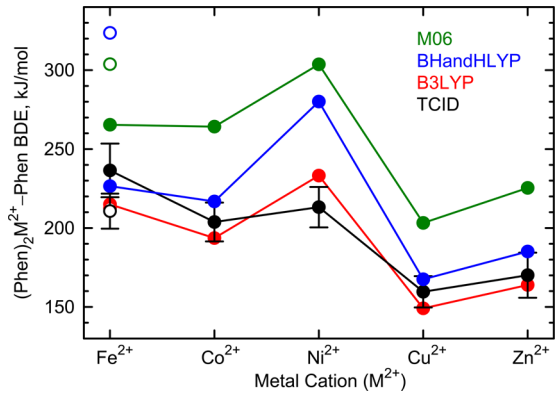

Figure 4. Comparison of theoretical and TCID measured $(Phen)_2M^{2+}$–Phen BDEs at 0 K (in kJ/mol), where M^{2+} = Fe^{2+}, Co^{2+}, Ni^{2+}, Cu^{2+}, and Zn^{2+}. Closed symbols represent dissociation from the ground-state reactant complex to ground-state products. For the $Fe^{2+}(Phen)_3$ complex, values for the singlet state are plotted as closed symbols, while open symbols represent BDEs obtained from dissociation of the quintet state of the $Fe^{2+}(Phen)_3$ complex. Theoretical BDEs determined at the B3LYP, BHandHLYP, and M06 levels of theory using the 6-311+G(2d,2p) basis set including ZPE and BSSE corrections. All values are taken from Table 2.

Comparison with Solution Phase. The third sequential binding energies determined here provide a measure of the intrinsic stability of the $M^{2+}(Phen)_3$ complexes in the gas phase and are found to follow the order $Cu^{2+} < Zn^{2+} < Co^{2+} < {}^5Fe^{2+} < Ni^{2+} < {}^1Fe^{2+}$ (see Table 2 and Figure 4). Binding constants for the stepwise coordination of M^{2+} cations with Phen in aqueous solution at 298 K and an ionic strength μ = 0.1 have been reported.[67] The values for log k_3 of the $M^{2+}(Phen)_3$ complexes in aqueous solution provide a quantitative measure of the stability of these complexes in solution and similar to that found here follow the order $Cu^{2+}(5.02) < Zn^{2+}(5.1) < Co^{2+}(6.28) < Ni^{2+}(7.9) < Fe^{2+}(10.3)$. While a highly quantitative comparison is not possible without considering solvent and counterion effects, the parallel stability order observed in the gas phase and in solution phase indicates that gas phase measurements can provide insight into solution phase relative stabilities in favorable cases.

Comparison between Experiment and Theory. Theoretical BDEs of the $M^{2+}(Phen)_3$ complexes derived from the B3LYP, BHandHLYP, and M06 levels of theory roughly parallel the measured BDEs but differ in absolute magnitude, Figure 4. The measured third sequential BDEs for all five $M^{2+}(Phen)_3$ complexes exhibit very good agreement with B3LYP theory. The mean absolute deviation (MAD) between B3LYP theory and experiment is 13.7 ± 6.7 kJ/mol for all five complexes when values for the singlet ground-state $Fe^{2+}(Phen)_3$ complex are used. The BDE of the singlet

dx.doi.org/10.1021/jp401711c | J. Phys. Chem. A 2013, 117, 4316–4330

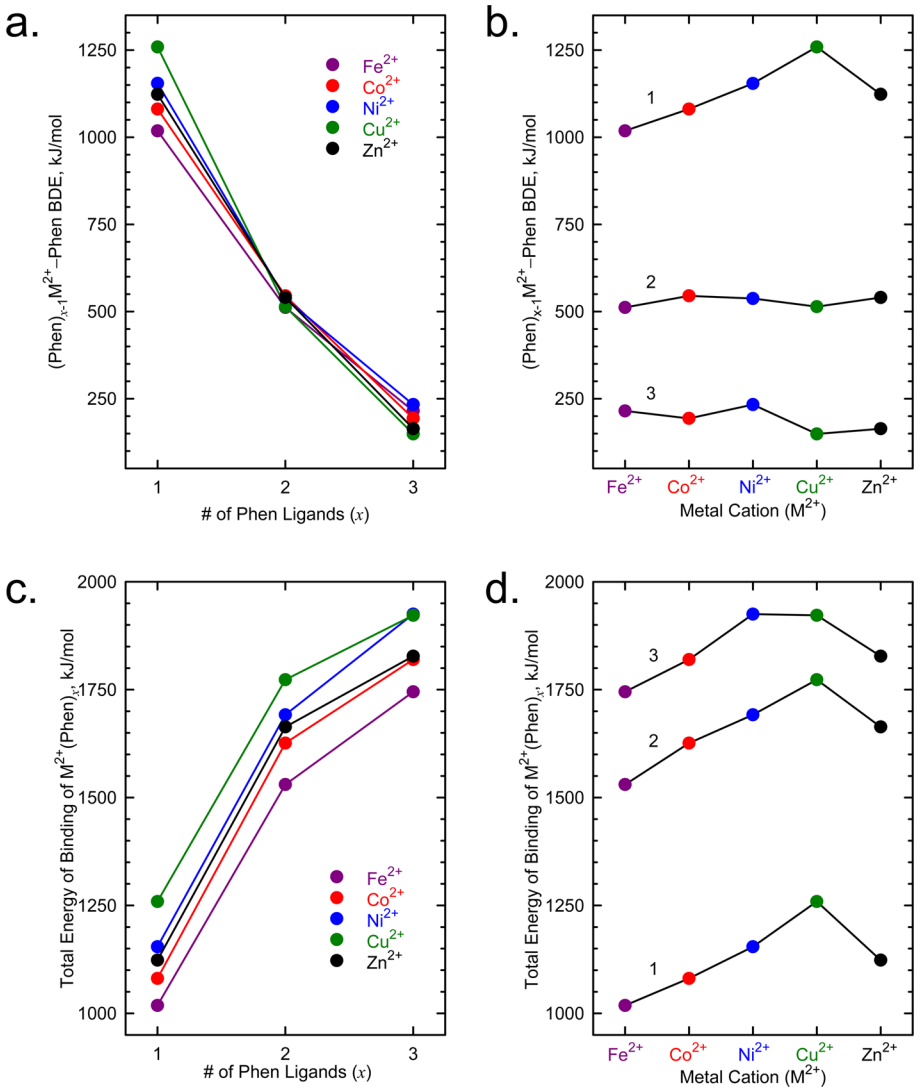

Figure 5. $(Phen)_{x-1}M^{2+}$–Phen BDEs where $M^{2+} = Fe^{2+}$, Co^{2+}, Ni^{2+}, Cu^{2+}, and Zn^{2+} as a function of the number of Phen ligands (x) and the metal cation, M^{2+}, parts a and b, respectively. Total energy of binding of $M^{2+}(Phen)_x$ complexes as a function of the number of Phen ligands (x) and the metal cation, M^{2+}, parts c and d, respectively. Theoretical BDEs at 0 K (in kJ/mol) determined at the B3LYP/6-311+G(2d,2p) level of theory including ZPE and BSSE corrections.

ground-state $Fe^{2+}(Phen)_3$ is 236.5 ± 17.0 kJ/mol, whereas the diabatic BDE of the excited-state $Fe^{2+}(Phen)_3$ is 210.7 ± 11.1 kJ/mol. The diabatic BDEs agree better with the B3LYP results. When values for the quintet excited state of the $Fe^{2+}(Phen)_3$ complex are used, the MAD reduces to 9.7 ± 6.7 kJ/mol. The measured third sequential BDEs for the Phen complexes to Co^{2+}, Cu^{2+}, Zn^{2+}, and Fe^{2+} (in its singlet state) also exhibit very good agreement with BHandHLYP theory, whereas the value calculated for the complex to Ni^{2+} and the quintet state of $Fe^{2+}(Phen)_3$ differ markedly from the measured BDEs. The MAD between BHandHLYP theory and experiment for all the five complexes is 22.3 ± 25.1 kJ/mol when the values for the singlet state of $Fe^{2+}(Phen)_3$ are used but reduces to 11.2 ± 3.4 kJ/mol when Ni^{2+} is not included. The MAD between BHandHLYP and experiment increases to 43.2 ± 45.7 kJ/mol when the values for the quintet state of $Fe^{2+}(Phen)_3$ are used. This implies that the singlet state of $Fe^{2+}(Phen)_3$ agrees much better with BHandHLYP than the quintet state of $Fe^{2+}(Phen)_3$ as well. The third sequential BDEs computed using M06 theory are systematically higher than BDEs obtained using the B3LYP and BHandHLYP theories by 42.5 ± 23.3 and 33.9 ± 33.6 kJ/mol, respectively. The larger binding energies found with M06 theory are consistent with the shorter M^{2+}–N bond lengths in the optimized geometries as compared to those for structures computed at the B3LYP and BHandHLYP levels of theory. The agreement between M06 theory and the measured BDEs for all of the complexes is very poor. M06 theory systematically overestimates the measured BDEs by 56.2 ± 22.3 kJ/mol when the singlet $Fe^{2+}(Phen)_3$ complex is used in the comparison. When the quintet state of $Fe^{2+}(Phen)_3$ is considered, the MAD increases to 68.6 ± 22.1 kJ/mol. Again, the BDE computed for the complex to Ni^{2+} and quintet state of $Fe^{2+}(Phen)_3$ exhibit the largest deviations from the measured values. The MAD between M06 theory and the TCID measured values reduces to 47.6 ± 13.1 kJ/mol when Ni^{2+} and the quintet state of the $Fe^{2+}(Phen)_3$ complex are not included. The average experimental uncertainty (AEU) in the measured BDEs is 13.3 ± 2.6 kJ/mol when the singlet $Fe^{2+}(Phen)_3$ complex is considered. The AEU values decrease to 12.1 ± 1.9 kJ/mol if the quintet state $Fe^{2+}(Phen)_3$ complex is

dx.doi.org/10.1021/jp401711c | J. Phys. Chem. A 2013, 117, 4316–4330

used. The AEU values are only slightly different than the MAD for B3LYP theory, but significantly smaller than the MADs for BHandHLYP and M06 theories. Thus, B3LYP theory provides the best description of the binding of the third ligand in the $M^{2+}(Phen)_3$ complexes.

Trends in the Sequential and Total BDEs of the $M^{2+}(Phen)_x$ Complexes. Trends in the B3LYP/6-311+G-(2d,2p) sequential and total binding energies of the $M^{2+}(Phen)_x$ complexes are illustrated in Figure 5 and summarized in Table 2. As illustrated in Figure 5 parts a and b, the strength of binding of the Phen ligands to the M^{2+} cations falls off rapidly with increasing ligation. The binding of the first Phen ligand is very strong and varies between 1018.3 and 1259.1 kJ/mol across these systems. The four N donor electrons of the Phen ligand stabilize the M^{2+} center greatly through electrostatic interactions. Hybridization of the M^{2+} cation also plays a major role in enhancing the binding energy of the first Phen ligand. Because the d_σ orbitals in all of the $M^{2+}(Phen)$ complexes are occupied, greater repulsion between the metal cations and the ligand occurs. $4s-3d_\sigma$ hybridization removes electron density along the metal−ligand bonding axis exposing the ligand to greater charge and allowing the ligand to approach the metal cation more closely (the $M^{2+}-N$ bond distances vary between 1.884 and 1.967 Å) and results in very strong binding of the first Phen ligand. The $M^{2+}(Phen)$ complexes are still electron deficient, and therefore binding of the second Phen ligand is still very strong. The strength of binding of the second Phen ligand varies between 511.8 and 545.2 kJ/mol, ∼40−50% as strong as binding of the first ligand. The weaker binding in the bis-complexes is the result of three effects, the decline in the effective positive charge retained by M^{2+} upon binding to the first ligand via two $M^{2+}-N$ dative interactions, repulsive interactions between the second Phen ligand and the occupied sd-hybridized orbital, and the repulsive interactions between the electron density of the first and second ligands. Binding of the second Phen overcomes much of the electron deficiency such that the $M^{2+}-N$ bond lengths increase by ∼0.1 Å and vary between 1.986 and 2.062 Å. Binding of the third Phen ligand is much weaker and varies between 149.1 and 233.2 kJ/mol, ∼14−20% as strong as binding to the first ligand, and the $M^{2+}-N$ bond lengths again increase and vary between 2.006 and 2.397 Å. The even weaker binding in the tris-complexes is again the result of three effects, the continued decline in the effective positive charge retained by M^{2+} upon binding to the first and second ligands via four $M^{2+}-N$ dative interactions, repulsive interactions between the first and second Phen ligands and the occupied sd-hybridized orbital, and the repulsive interactions between the electron density of the three Phen ligands.

With each Phen ligand bound to the M^{2+} metal center, the electrostatic contributions to the binding decrease because the effective charge retained by the metal cation decreases as more electrons are added to the metal center. Similarly, ligand−ligand repulsive interactions between the Phen ligands increase upon sequential ligation, leading to weaker binding. These effects act in concert to lengthen the $M^{2+}-N$ bond lengths with increasing ligation. Notably, the variation in the BDEs of the first ligand to all five metal cations is largest, 240.8 kJ/mol. This large variation directly reflects the differences in stabilization the metal cations achieve via sd hybridization, which increases with increasing d orbital occupation. The second sequential BDEs exhibit the least variation, 33.4 kJ/mol, primarily because sd hybridization effects diminish greatly as binding of the second Phen ligand produces much greater repulsion with the occupied sd hybrid orbital. The variation in the third sequential BDEs is intermediate, 84.1 kJ/mol. The larger variation in the BDEs across the tris-complexes arises because of spin crossover in the Fe^{2+} system and slight Jahn−Teller effects in the Co^{2+} and significant Jahn−Teller effects in the Cu^{2+} systems.

The evolution in the nature of the binding in the $M^{2+}(Phen)_x$ complexes as a function of ligation is clearly seen in the dissociation behavior of these complexes. In all of the $M^{2+}(Phen)_3$ complexes, the most prominent fragmentation channel is the loss of an intact Phen ligand. The measured BDEs of the $M^{2+}(Phen)_3$ complexes are all <240 kJ/mol, weaker than a typical C−C covalent bond, >400 kJ/mol.[66] Thus, their CID behavior indicates that the nature of the binding of the third ligand in the $M^{2+}(Phen)_3$ complexes is predominantly noncovalent. In comparison with the $M^{2+}(Phen)_3$ complexes, the BDEs calculated for the $M^{2+}(Phen)_2$ complexes are >400 kJ/mol, implying that the binding of the second Phen ligand is more covalent in nature. As a result, the CID behavior of the $M^{2+}(Phen)_2$ complexes is much richer and provides an opportunity to probe the metal-to-ligand and ligand-to-metal charge transfer behavior in much greater detail. The BDEs of the $M^{2+}(Phen)$ complexes are calculated to be >1000 kJ/mol suggesting that covalent interactions dominate the binding. However, the high electron deficiency of these complexes makes these complexes too reactive to generate in sufficient intensity to enable studies of their CID behavior.

Periodic Trends in the Sequential BDEs of the $M^{2+}(Phen)_x$ Complexes. Periodic trends in the BDEs of the monocomplexes are shown in Figure 5, parts a and b. The $M^{2+}-Phen$ BDEs follow the order $Fe^{2+} < Co^{2+} < Zn^{2+} < Ni^{2+} < Cu^{2+}$. This trend is explained by the relative sizes of the metal cations, which have ionic radii of 0.76, 0.74, 0.73, 0.72, and 0.72 Å for Fe^{2+}, Co^{2+}, Ni^{2+}, Cu^{2+}, and Zn^{2+}, respectively.[54,55] The variation in metal cation radii roughly parallels the $M^{2+}-N$ bond lengths, which decrease from Fe^{2+} to Cu^{2+} as the d-orbital occupation increases. This trend is also inversely correlated with the second ionization energies (IEs) of the metal: 16.19, 17.08, 18.17, and 20.29 eV for Fe, Co, Ni, and Cu, respectively.[68] The ionic radii, $M^{2+}-N$ bond lengths, and the second IEs serve as guides to the magnitude of the electrostatic interactions involved in these complexes and determines how closely the Phen ligand can approach the metal center. Considering the $M^{2+}-N$ bond lengths, ionic radii, and second IEs, the trend in the BDEs, $Cu^{2+}(Phen) > Zn^{2+}(Phen)$ is reasonable. However, no simple correlation exists because Zn has a higher second IE (17.96 eV) than Fe (16.19 eV) and Co (17.08 eV), but Zn^{2+} has a smaller ionic radius than Fe^{2+}, Co^{2+}, and Ni^{2+}. The second sequential BDEs, $(Phen)M^{2+}-Phen$, increase in the order $Fe^{2+} < Cu^{2+} < Co^{2+} < Zn^{2+} < Ni^{2+}$. The stability order has changed immensely for $Cu^{2+}(Phen)_2$ due to increased ligand−ligand repulsion as two Phen ligands position themselves around the very small Cu^{2+} cation adopting a geometry closer to square planar to minimize repulsion with the occupied sd hybrid orbital and also suggesting that Jahn−Teller effects are beginning to take effect in the bis-complexes. Overall, the sequential BDEs of the $M^{2+}(Phen)_2$ complexes remain closely related to the minor structural differences found for these complexes. The third sequential BDEs, $(Phen)_2M^{2+}-Phen$, follow the order $Cu^{2+} < Zn^{2+} < Co^{2+} < Fe^{2+} < Ni^{2+}$. The trend in the third sequential BDEs differs from that observed for binding of the first and second ligands. The relative BDEs

dx.doi.org/10.1021/jp401711c | J. Phys. Chem. A 2013, 117, 4316−4330

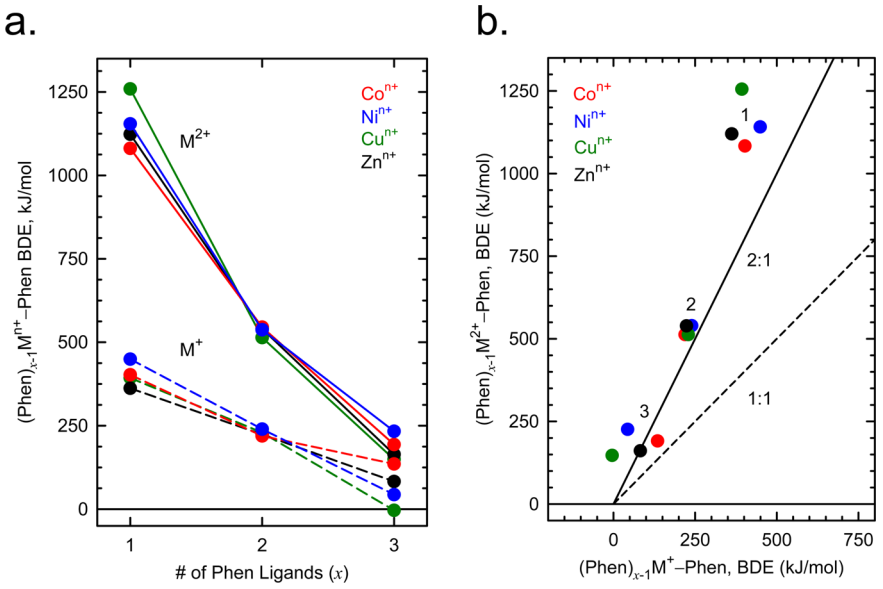

Figure 6. Comparison of B3LYP/6-311+G(2d,2p) calculated BDEs of the $M^{n+}(Phen)_x$ complexes as a function of the number of Phen ligands (x) and charge (n+), parts a and b, respectively. Values for M^{2+} are taken from Table 2 and include ZPE and BSSE corrections. Values for M^+ are taken from refs 22−25.

vary primarily because the Cu^{2+} complexes shift from being the most strongly bound when x = 1 to the least strongly bound when x = 3. This anomaly in the BDEs is a consequence of Jahn−Teller effects, by which the $Cu^{2+}(Phen)_3$ complex exhibits pronounced tetragonal distortions leading to a weaker third sequential BDE. Changes in the trends in the BDEs calculated for the Co^{2+} complex due to Jahn−Teller distortions is slight. Fe^{2+}, on the other hand, exhibits the weakest binding energy among the monocomplexes, while the tris-complex exhibits a much stronger binding energy. As the extent of ligation increases, the order of stabilities changes drastically with the $Fe^{2+}(Phen)_3$ becoming more stable. This anomalous stability of the $Fe^{2+}(Phen)_3$ complex arises due to the formation of a spin-paired complex. Under the stronger field splitting provided by the three Phen ligands, the electrons become spin paired, so that a more stable diamagnetic complex results. This results in the d_{σ^*} orbitals being empty, and hence less repulsion with the Phen ligand, and increasing the BDE of the $Fe^{2+}(Phen)_3$ complex.

Periodic Trends in the Total BDEs of the $M^{2+}(Phen)_x$ Complexes. The trends in the total binding energies of the $M^{2+}(Phen)_x$ complexes as a function of the number of Phen ligands interacting with the M^{2+} cation are shown in Figure 5, parts c and d. The total binding energy obviously increases as the number of Phen ligands increases. The binding energy of the first Phen ligand varies between 1018.3 and 1259.1 kJ/mol. The total binding energies for the bis- and tris-complexes are ∼1.5 and ∼1.7 times as strong as those for the monocomplexes, respectively. The total binding energies increase sharply from x = 1 to x = 2, and less dramatically from x = 2 to x = 3. The trends in the total binding energies for the five metal complexes roughly parallel each other. The total energy of binding follows the order $Cu^{2+} > Ni^{2+} > Zn^{2+} > Co^{2+} > Fe^{2+}$. This trend can be explained by the three most important factors that control the strength of binding in these $M^{2+}(Phen)_x$ complexes, i.e., sd hybridization of the metal cation, Jahn−Teller effects, and ligand−ligand repulsion. sd Hybridization plays a key role when binding the first ligand to the M^{2+} cation. When binding the second Phen ligand, stabilization from sd hybridization is lost, while Jahn−Teller effects become pronounced for the $Cu^{2+}(Phen)_2$ complex as the ligands attempt to mimimize repulsion with the occupied sd-hybridized orbital by reducing the ∠$NM^{2+}NC$ dihedral angles between the Phen ligands. Upon binding of the third ligand, Jahn−Teller effects become the dominant factor, strongly influencing the structure and binding in the $Cu^{2+}(Phen)_3$ complex. The effects of the spin change of the $Fe^{2+}(Phen)_x$ systems upon binding of the third Phen ligand helps to provide additional stabilization to the tris-complex, but the lesser stabilization achieved from sd hybridization of the x = 1 complex leads to Fe^{2+} exhibiting the weakest total binding energy among the tris-complexes.

Comparison of the BDEs of $M^{2+}(Phen)_x$ and $M^+(Phen)_x$. The sequential bond dissociation energies (BDEs) of the $M^{2+}(Phen)_x$ complexes, where x = 1−3, are compared to those of the analogous $M^+(Phen)_x$ complexes in Figure 6a.[22−25] As can be seen in the figure, the sequential BDEs decrease monotonically as the number of ligands increases from one to three for the complexes to both the M^{2+} and M^+ cations. The rapid decrease in the sequential BDEs for both the $M^{2+}(Phen)_x$ and $M^+(Phen)_x$ complexes arises because the electrostatic contributions to the binding decrease rapidly upon sequential ligation because each Phen ligand provides two N donor interactions such that the charge retained by the metal cation decreases rapidly. In both cases, an increase in M^{n+}−N bond distances as the size of the complex increases is observed. For example, the Zn^+−N bond lengths of the $Zn^+(Phen)_x$ complexes increase from 2.057 to 2.010 to 2.191 Å, whereas Zn^{2+}−N bond lengths of the $Zn^{2+}(Phen)_x$ increase from 1.913 to 2.023 to 2.193 Å as x increases from 1 to 3, respectively. In contrast, the BDEs decrease from 362.2 to 223.7 to 82.6 kJ/mol for the $Zn^+(Phen)_x$ complexes, whereas those of the $Zn^{2+}(Phen)_x$ decrease from 1120.2 to 539.0 to 161.0 kJ/mol as x increases from 1 to 3, respectively. The difference in the Zn^{n+}−N bond distances is greater in the mono-complexes and decreases as the number of ligands increases. Ligand−ligand repulsion also contributes to the

dx.doi.org/10.1021/jp401711c | J. Phys. Chem. A 2013, 117, 4316−4330

decrease in the sequential BDEs. The BDEs are larger for the M^{2+} complexes as compared to the analogous M^+ complexes. The ratio between the BDEs of the doubly charged to the singly charged complexes decreases as the number of ligand increases and is roughly 2.95:1 for the mono-, 2.46:1 for the bis-, and 1.70:1 for the tris-complexes. In spite of these large differences in the binding energies, the structural differences between the analogous $M^{2+}(Phen)_x$ and $M^+(Phen)_x$ complexes are very nominal. For example, the difference between the bond lengths found in $Zn^+(Phen)_x$ compared to their analogous $Zn^{2+}(Phen)_x$ complexes is quite small except for the monocomplexes. The differences in the BDEs of these complexes are largely the result of electrostatics; i.e., the ion−dipole and ion−induced dipole interactions are twice as strong for the M^{2+} complexes as those to M^+ when the M^{n+}−N bond lengths are preserved. However, the M^{2+} cations are smaller than the M^+ cations, and hence the binding interactions with the Phen ligand are more than twice as strong because the Phen ligand can approach the M^{2+} cation more closely. The difference in BDEs between the analogous doubly and singly charged complexes becomes narrower as the number of ligands increases as illustrated in Figure 6b. Thus, it is clear that additional ligands are required to stabilize the M^{2+} cations to a point where the energies become comparable to those of the complexes to the M^+ cations.

The trends in the sequential BDEs of these $M^{n+}(Phen)_x$ complexes can be understood in terms of several competing factors including electrostatic interactions, metal−ligand hybridization, and ligand−ligand repulsion. The metal−ligand bonding interactions in the $M^{2+}(Phen)_x$ and $M^+(Phen)_x$ complexes are similar. The $Co^{2+}(d^7)$, $Ni^{2+}(d^8)$, $Co^+(d^8)$, $Cu^{2+}(d^9)$, and $Ni^+(d^9)$ cations are partially occupied. The $Zn^{2+}(d^{10})$ is isoelectronic with the $Cu^+(d^{10})$ cation, which is fully occupied, whereas the $Zn^+(4s^13d^{10})$ cation has an extra electron in its s orbital. When these cations form bonds with Phen ligands π-back-donation is expected to increase from Co^{2+} to Zn^{2+} and further from Co^+ to Zn^+ across the period. Most favorable π-back-donation arises when there is a filled d orbital because the metal cation overlaps better with the π^* orbital of the planar π network of Phen. Because the d_{σ^*} orbitals in all of the $M^{n+}(Phen)_x$ complexes are occupied, greater repulsion between the metal cation and the ligands is expected. Even more repulsion is expected for the $Zn^+(Phen)_x$ complexes because the s orbital is occupied. In the $M^{n+}(Phen)$ monocomplexes, 4s−3d hybridization effectively removes electron density from the metal−ligand axis by placing the electron density in a hybridized orbital that is perpendicular to the bonding axis for all of the metal cations except Zn^+. This results in a higher BDE for all of the monocomplexes. The enhancements in binding increase across the period with increasing orbital occupation. In the case of $Zn^+(Phen)$, sp polarization plays a similar role as sd hybridization and removes electron density from the metal−ligand axis by placing the electron density in a hybridized orbital oriented 180° away from the bonding axis. However, sp polarization produces less stabilization than sd hybridization as the orbitals lie higher in energy. The decline in the effective positive charge and repulsive interactions between electron densities further diminish the BDEs. Hence the differences in the binding patterns observed in the $M^{n+}(Phen)_x$ complexes are dominated by the charge. Figure 7 shows the trends in the third sequential BDEs for the Phen complexes of M^{2+} and M^+. The binding in the d^8, d^9, and d^{10} complexes is roughly parallel for the M^{2+} and

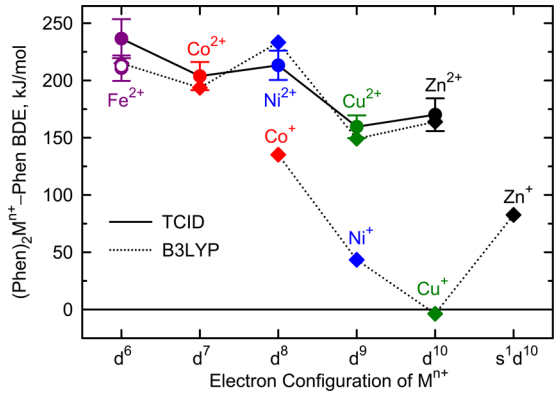

Figure 7. Periodic trends in the TCID measured and calculated $(Phen)_2M^{n+}$−Phen BDEs at 0 K (in kJ/mol), where M = Fe, Co, Ni, Cu, and Zn and n = 1 and 2. Closed symbols represent dissociation from the ground-state reactant complex to ground-state products. For the $Fe^{2+}(Phen)_3$ complex, values for the singlet state are plotted as closed symbols, while the open symbols represent BDEs obtained from dissociation of the quintet state of the $Fe^{2+}(Phen)_3$ complex. Calculated values determined at the B3LYP/6-311+G(2d,2p) level of theory including ZPE and BSSE corrections. Values for M^{2+} are taken from Table 2. Values for M^+ are taken from refs 22−25.

M^+ complexes. However, the $Cu^+(Phen)_3$ complex is actually calculated to be unbound at room temperature. This is supported by the Gibbs free energy at 298 K (−56.7 kJ/mol) for the loss of Phen from the $Cu^+(Phen)_3$ complex, suggesting that dissociation would be spontaneous. Appreciable ion beams of any of the $M^+(Phen)_3$ complexes were not obtained because their internal energies at room temperature exceed the BDEs.[22−25] However, our ability to generate intense ion beams of $Cu^{2+}(Phen)_3$ and the other $M^{2+}(Phen)_3$ complexes and measure their CID behavior clearly establishes that these species are bound, and loss of a single Phen ligand from these complexes is endothermic.

CONCLUSIONS

The kinetic energy dependences of the CID of the tris-ligated complexes of the late first-row divalent transition metal cations to Phen, $M^{2+}(Phen)_3$, with Xe are examined in a guided ion beam tandem mass spectrometer. The dominant dissociation pathway for all complexes is loss of an intact Phen ligand. The thresholds for these processes are determined after consideration of the effects of the internal energy distribution of the reactant $M^{2+}(Phen)_3$ complexes,[35] multiple collisions with Xe,[36] and lifetime effects.[26,51,69] Sequential BDEs of the $M^{2+}(Phen)_x$ complexes are determined at the B3LYP/6-311+G(2d,2p)//B3LYP/6-31G*, BHandHLYP/6-311+G(2d,2p)//BHandHLYP/6-31G*, and M06/6-311+G(2d,2p)//M06/6-31G* levels of theory. The computed sequential BDEs are highly parallel but differ in absolute magnitude. BDEs computed using the M06 functional are the strongest, BHandHLYP values are intermediate, whereas B3LYP produces the weakest BDEs. Very good agreement between the B3LYP theoretically calculated and TCID experimentally determined BDEs is found, suggesting that the B3LYP functional is capable of accurately describing the binding in these tris-complexes. The present results suggest that the bonding in the $M^{2+}(Phen)_x$ complexes is dominantly electrostatic. Comparison of the $M^{2+}(Phen)_x$ to the analogous $M^+(Phen)_x$ complexes indicates that the charge (or oxidation state) of the metal cation is the dominant factor contributing to the differences in the strength

dx.doi.org/10.1021/jp401711c | J. Phys. Chem. A 2013, 117, 4316−4330

of binding among these complexes. The strength of binding is also found to depend on the electron configuration of the metal cation; however, differences in the strength of binding are much smaller for cations of the same charge.

■ ASSOCIATED CONTENT

Supporting Information

Complete citation for refs 37 and 38; tables of vibrational frequencies, average vibrational energies at 298 K, and rotational constants for the neutral Phen ligand and $M^{2+}(Phen)_x$ complexes in their ground-state conformations; table of relative energies computed for the various possible spin states of the $M^{2+}(Phen)_x$ complexes at 0 K in kJ/mol where M^{2+} = Fe^{2+}, Co^{2+}, and Ni^{2+}; tables of geometrical parameters of the BHandHLYP/6-31G* and M06/6-31G* ground-state structures of the Phen ligand and $M^{2+}(Phen)_x$ complexes; figures showing cross sections for CID of $M^{2+}(Phen)_3$ with Xe as well as empirical fits to the primary $M^{2+}(Phen)_2$ product channels for M^{2+} = Fe^{2+}, Co^{2+}, and Ni^{2+}; figures showing the average M^{2+}−N bond distances in B3LYP/6-31G* optimized $M^{2+}(Phen)_x$, x = 1−3, complexes as a function of the metal cation as compared to the ionic radii of the bare metal cation, M^{2+}; figures showing the ground-state structures of the $M^{2+}(Phen)_x$ complexes, where M^{2+} = Fe^{2+}, Co^{2+}, and Ni^{2+} and x = 1−3. This material is available free of charge via the Internet at http://pubs.acs.org.

■ AUTHOR INFORMATION

Notes

The authors declare no competing financial interest.

■ ACKNOWLEDGMENTS

This work is supported by the National Science Foundation, Grant CHE-0911191. The authors thank WSU C&IT for computer time and support. We also thank Dr. Cliff Frieler for technical support.

■ REFERENCES

(1) Costello, J. F.; Davies, S. G.; McNally, D. The Conformational Analysis of Phosphine Ligands in Organometallic Complexes. Part 2. Triphenylphosphine Coordinated to Achiral and Prochiral Octahedral Metal Centers. *J. Chem. Soc., Perkin Trans. 2* **1999**, 465−474.

(2) Noyori, R.; Takaya, H. BINAP: An Efficient Chiral Element for Asymmetric Catalysis. *Acc. Chem. Res.* **1990**, *23*, 345−350.

(3) Brandt, W. W.; Dwyer, F. P.; Gyarfas, E. C. Chelate Complexes of 1,10-Phenanthroline and Related Compounds. *Chem. Rev.* **1954**, *54*, 959−1017.

(4) Summers, L. A. The Phenanthrolines. *Adv. Heterocycl. Chem.* **1978**, *22*, 1−69.

(5) Holyer, R. H.; Hubbard, C. D.; Kettle, S. F. A.; Wilkins, R. G. The Kinetics of Replacement Reactions of Complexes of The Transition Metals with 1,10-Phenanthroline and 2,2′-Bipyridine. *Inorg. Chem.* **1965**, *4*, 929−935.

(6) Graham, B. *Six-Membered Heterocyclic Nitrogen Compounds with Three Condensed Rings*; Wiley-Interscience: New York. 1958; pp 386−456.

(7) Keipert, S. J.; Knobler, C. B.; Cram, D. J. Host−Guest Complexation. 43. Synthesis and Binding Properties of a Macrocycle Composed of Two Phenanthrolines and Two Sulfonamide Units. *Tetrahedron* **1987**, *43*, 4861−4874.

(8) Chandler, C. J.; Deady, L. W.; Reiss, J. A. Macrocyclic Polyether and Polythioether Diesters and Dithioesters from 1,10-Phenanthroline-2,9-Dicarboxylic Acid. *J. Heterocycl. Chem.* **1986**, *23*, 1327−1330.

(9) Gladiali, S.; Chelucci, G.; Soccolini, F.; Delogu, G.; Chessa, G. Optically Active Phenanthrolines in Asymmetric Catalysis. II. Enantioselective Transfer Hydrogenation of Acetophenone by Rhodium-Alkylphenanthroline Catalysts. *J. Organomet. Chem.* **1989**, *370*, 285−294.

(10) Gladiali, S.; Pinna, L.; Delogu, G.; De Martin, S.; Zassinovich, G.; Mestroni, G. Optically Active Phenanthrolines in Asymmetric Catalysis. III. Highly Efficient Enantioselective Transfer Hydrogenation of Acetophenone by Chiral Rhodium/3-Alkyl Phenanthroline Catalysts. *Tetrahedron: Asymmetry* **1990**, *1*, 635−648.

(11) Schoffers, E. Reinventing Phenanthroline Ligands—Chiral Derivatives for Asymmetric Catalysis. *Eur. J. Org. Chem.* **2003**, *7*, 1145−1152.

(12) Chelluci, G.; Thummel, R. P. Chiral 2,2′-Bipyridines, 1,10-Phenanthrolines, and 2,2′:6′,2″-Terpyridines: Syntheses and Applications in Asymmetric Homogeneous Catalysis. *Chem. Rev.* **2002**, *102*, 3129−3170.

(13) Puglisi, A.; Benaglia, M.; Annunziata, R.; Bologna, A Enantiomerically Pure Phenanthroline- or Bipyridine-Containing Macrocycles: A New Class of Ligands for Asymmetric Catalysis. *Tetrahedron Lett.* **2003**, *44*, 2947−2951.

(14) Gladysz, J. A.; Boone, B. J. Chiral Recognition in π Complexes of Alkenes, Aldehydes, and Ketones with Transition Metal Lewis Acids; Development of a General Model for Enantioface Binding Selectivities. *Angew. Chem., Int. Ed. Engl.* **1997**, *36*, 551−583.

(15) Hollis, T. K.; Odenkirk, W.; Robinson, N. P.; Whelan, J.; Bosnich, B. Homogeneous Catalysis. Transition Metal Based Lewis Acid Catalysts. *Tetrahedron* **1993**, *49*, 5415−5430.

(16) Davenport, A. J.; Fawcett, J.; Lad, L.; Russell, R. R. Synthesis of Chiral Half-Sandwich Rhodium Oxazoline Complexes and Their Use as Asymmetric Diels−Alder Catalysts. *Chem. Commun.* **1997**, 2347−2348.

(17) Irving, H.; Mellor, D. H. Stability of Metal Complexes of 1,10-Phenanthroline and Its Analogs. I. 1,10-Phenanthroline and 2,2′-Bipyridine. *J. Chem. Soc.* **1962**, 5222−5237.

(18) Irving, H.; Mellor, D. H. Stability of Metal Complexes of 1,10-Phenanthroline and Its Analogs. II. 2-Methyl- and 2,9-Dimethylphenanthroline. *J. Chem. Soc.* **1962**, 5237−5245.

(19) McBryde, W. A. E.; Brisbin, D. A.; Irving, H. Stability of Metal Complexes of 1,10-Phenanthroline and Its Analogs. III. 5-Methyl-1,10-Phenanthroline. *J. Chem. Soc.* **1962**, 5245−5253.

(20) Irving, H. M.; Williams, R. J. P. Stability of Transition Metal Complexes. *J. Chem. Soc.* **1953**, 3192−3210.

(21) Irving, H. M.; Cabell, M. J.; Mellor, D. H. Steric Hindrance in Analytical Chemistry. II. The Interaction of Ferrous Salts with 2-Substituted 1,10-Phenanthrolines. *J. Chem. Soc.* **1953**, 3417−3426.

(22) Rannulu, N. S.; Rodgers, M. T. Noncovalent Interactions of Cu^+ with *N*-Donor Ligands (Pyridine, 4,4′-Dipyridyl, 2,2′-Dipyridyl, and 1,10-Phenanthroline): Collision-Induced Dissociation and Theoretical Studies. *J. Phys. Chem. A* **2007**, *111*, 3465−3479.

(23) Rannulu, N. S.; Rodgers, M. T. Noncovalent Interactions of Zn^+ with *N*-Donor Ligands (Pyridine, 4,4′-Dipyridyl, 2,2′-Dipyridyl, and 1,10-Phenanthroline): Collision-Induced Dissociation and Theoretical Studies. *J. Phys. Chem. A* **2012**, *116*, 1319−1332.

(24) Rannulu, N. S.; Rodgers, M. T. Noncovalent Interactions of Ni^+ with *N*-Donor Ligands (Pyridine, 4,4′-Dipyridyl, 2,2′-Dipyridyl, and 1,10-Phenanthroline): Collision-Induced Dissociation and Theoretical Studies. *J. Phys. Chem. A* **2009**, *113*, 4534−4548.

(25) Rannulu, N. S. Noncovalent Interactions between Metal Ions and Analytically and Biologically Relevant Molecules: Collision-Induced Dissociation and Theoretical Studies. Doctoral Dissertation, Wayne State University, 2008; pp 1−383.

(26) Rodgers, M. T.; Ervin, K. M.; Armentrout, P. B. Statistical Modeling of Collision-Induced Dissociation Thresholds. *J. Chem. Phys.* **1997**, *106*, 4499−4508.

(27) Gillard, R. D.; Hill, R. E.; Maskill, R. J. Optically Active Coordination Compounds. XX. Reactions of 1,10-Phenanthroline Coordinated to Cobalt(III). *J. Chem. Soc. A* **1970**, *9*, 1447−1451.

(28) Hunt, H. R., Jr. Synthesis and Properties of an Optically Active Complex: A Polarimeter Experiment for General Chemistry. *J. Chem. Educ.* **1977**, *54*, 710−711.

(29) Rodgers, M. T. Substituent Effects in the Binding of Alkali Metal Ions to Pyridines, Studied by Threshold Collision-Induced Dissociation and Ab Initio Theory: The Methylpyridines. *J. Phys. Chem. A* **2001**, *105*, 2374−2383.
(30) Chen, Y.; Rodgers, M. T. Structural and Energetic Effects in the Molecular Recognition of Protonated Peptidomimetic Bases by 18-Crown-6. *J. Am. Chem. Soc.* **2012**, *134*, 2313−2324.
(31) Teloy, E.; Gerlich, D. Integral Cross Sections for Ion−Molecule Reactions. I. The Guided Beam Technique. *Chem. Phys.* **1974**, *4*, 417−427.
(32) Gerlich, D. Inhomogeneous RF Fields: A Versatile Tool for the Study of Processes with Slow Ions. *Adv. Chem. Phys.* **1992**, *82*, 1−176.
(33) Dalleska, N. F.; Honma, K.; Armentrout, P. B. Stepwise Solvation Enthalpies of Protonated Water Clusters: Collision-Induced Dissociation as an Alternative to Equilibrium Studies. *J. Am. Chem. Soc.* **1993**, *115*, 12125−12131.
(34) Aristov, N.; Armentrout, P. B. Collision-Induced Dissociation of Vanadium Monoxide Ion. *J. Phys. Chem.* **1986**, *90*, 5135−5140.
(35) Ervin, K. M.; Armentrout, P. B. Translational Energy Dependence of $Ar^+ + XY \rightarrow ArX^+ + Y$ (XY = H_2, D_2, HD) from Thermal to 30 eV. *J. Chem. Phys.* **1985**, *83*, 166−189.
(36) Dalleska, N. F.; Honma, K.; Sunderlin, L. S.; Armentrout, P. B. Solvation of Transition Metal Ions by Water. Sequential Binding Energies of $M^+(H_2O)_x$ (x = 1−4) for M = Ti to Cu Determined by Collision-Induced Dissociation. *J. Am. Chem. Soc.* **1994**, *116*, 3519−3528.
(37) Frisch, M. J.; Trucks, G. W.; Schlegel, H. B.; Scuseria, G. E.; Robb, M. A.; Cheeseman, J. R.; Montgomery, J. A., Jr.; Vreven, T.; Kudin, K. N.; Burant, J. C.; et al. *Gaussian03*; Gaussian Inc.: Wallingford, CT, 2004.
(38) Frisch, M. J.; Trucks, G. W.; Schlegel, H. B.; Scuseria, G. E.; Robb, M. A.; Cheeseman, J. R.; Scalmani, G.; Barone, V.; Mennucci, B.; Petersson, G. A.; et al. *Gaussian09*; Gaussian Inc.: Wallingford, CT, 2009.
(39) Meng, L.; Hu, A.; Pang, R.; Lin, Z. Extensive Computational Study on Coordination of Transition Metal Cations and Water Molecules to Glutamic Acid. *J. Phys. Chem. A* **2012**, *116*, 7177−7188.
(40) Zhao, Y.; Truhlar, D. G. The M06 Suite of Density Functionals for Main Group Thermochemistry, Thermochemical Kinetics, Noncovalent Interactions, Excited States, and Transition Elements: Two New Functionals and Systematic Testing of Four M06-Class Functionals and 12 Other Functionals. *Theor. Chem. Acc.* **2008**, *120*, 215−241.
(41) Becke, A. D. Density-Functional Thermochemistry. III. The Role of Exact Exchange. *J. Chem. Phys.* **1993**, *98*, 5648−5652.
(42) Lee, C.; Yang, W.; Parr, R. G. Development of the Colle−Salvetti Correlation-Energy Formula into a Functional of the Electron Density. *Phys. Rev. B* **1988**, *37*, 785−789.
(43) Foresman, J. B.; Frisch, Æ. *Exploring Chemistry with Electronic Structure Methods*, 2nd ed.; Gaussian: Pittsburgh, PA, 1996; p 64.
(44) Boys, S. F.; Bernardi, F. The Calculation of Small Molecular Interactions by the Differences of Separate Total Energies. Some Procedures with Reduced Errors. *Mol. Phys.* **1970**, *19*, 553−566.
(45) van Duijneveldt, F. B.; van Duijneveldt de Rijdt, J. G. C. M.; van Lenthe, J. H. State of the Art in Counterpoise Theory. *Chem. Rev.* **1994**, *94*, 1873−1885.
(46) Nelson, R. D.; Lide, D. R.; Maryott, A. A. National Standards References Data Series 10; *National Bureau of Standards*: Washington, DC; 1967.
(47) Muntean, F.; Armentrout, P. B. Guided Ion Beam Study of Collision-Induced Dissociation Dynamics: Integral and Differential Cross Sections. *J. Chem. Phys.* **2001**, *115*, 1213−1228.
(48) Beyer, T. S.; Swinehart, D. F. Algorithm 448: Number of Multiple-Restricted Partitions. *Commun. Assoc. Comput. Machines* **1973**, *16*, 379.
(49) Stein, S. E.; Rabinovitch, B. S. Accurate Evaluation of Internal Energy Level Sums and Densities Including Anharmonic Oscillators and Hindered Rotors. *J. Chem. Phys.* **1973**, *58*, 2438−2445.
(50) Stein, S. E.; Rabinovitch, B. S. On the Use of Exact State Counting Methods in RRKM Rate Calculations. *Chem. Phys. Lett.* **1977**, *49*, 183−188.
(51) Khan, F. A.; Clemmer, D. E.; Schultz, R. H.; Armentrout, P. B. Sequential Bond Energies of Chromium Carbonyls $(Cr(CO)_x^+$, x = 1−6). *J. Phys. Chem.* **1993**, *97*, 7978−7987.
(52) Chesnavich, W. J.; Bowers, M. T. Theory of Translationally Driven Reactions. *J. Phys. Chem.* **1979**, *83*, 900−905.
(53) Armentrout, P. B.; Simons, J. Understanding Heterolytic Bond Cleavage. *J. Am. Chem. Soc.* **1992**, *114*, 8627−8633.
(54) Shannon, R. D. Revised Effective Ionic Radii and Systematic Studies of Interatomic Distances in Halides and Chalcogenides. *Acta Crystallogr.* **1976**, *A32*, 751−767.
(55) Jia, Y. Q. Crystal Radii and Effective Ionic Radii of the Rare Earth Ions. *J. Solid Sate Chem.* **1991**, *95*, 184−187.
(56) Reiher, M. Theoretical Study of the $Fe(Phen)_2(NCS)_2$ Spin-Crossover Complex with Reparametrized Density Functionals. *Inorg. Chem.* **2002**, *41*, 6928−6935.
(57) Swart, M. Accurate Spin-State Energies for Iron Complexes. *J. Chem. Theory Comput.* **2008**, *4*, 2057−2066.
(58) Tanabe, Y.; Sugano, S. The Absorption Spectra of Complex Ions. I. *J. Phys. Soc. Jpn.* **1954**, *9*, 753−766.
(59) Fisher, D. C.; Drickamer, H. G. Effect of Pressure on the Spin State of Iron in Ferrous Phenanthroline Compounds. *J. Chem. Phys.* **1971**, *54*, 4825−4837.
(60) Bargerum, C. B.; Drickamer, H. G. Effect of Pressure on the Electronic Structure of Complexes of Ferrous Iron with Substituted Phenanthrolines. *J. Chem. Phys.* **1971**, *55*, 3471−3482.
(61) Goodwin, H. A.; Sylva, R. N. Magnetic Properties of the Tris(2-Methyl-1,10-Phenanthroline)Iron(II) Ion. *Aust. J. Chem.* **1968**, *21*, 83−90.
(62) Harris, C. M.; Kokot, S.; Patil, H. R. H.; Sinn, E.; Wong, H. High-and Low-Spin Complexes with Similar Ligands. II. Iron(II) Complexes with Sterically Hindered Analogs of 2,2′-Bipyridyl. *Austr. J. Chem.* **1972**, *25*, 1631−1643.
(63) Konig, E.; Ritter, G.; Spiering, H.; Kremer, S.; Madeja, K.; Rosenkranz, A. Slow Electronic Relaxation in 5T2−1A1 Spin Equilibriums of Tris(2-Methyl-1,10-Phenanthroline)Iron(II) Complexes. Moessbauer Effect Study. *J. Chem. Phys.* **1972**, *56*, 3139−3145.
(64) Reiff, W. M.; Long, G. J. Nature of the Electronic Ground State in Tris(2-ChloroPhenanthroline)Iron(II) Perchlorate and Related Complexes. *Inorg. Chem.* **1974**, *13*, 2150−2153.
(65) Collins, R. L.; Pettit, R.; Baker, W. A. Moessbauer Studies of Iron Organometallic Complexes. III. Octahedral Complexes. *J. Inorg. Nucl. Chem.* **1966**, *28*, 1001−1010.
(66) Carey, F. A.; Giuliano, R. M. *Organic Chemistry*, 8th ed.; McGraw-Hill: New York, 2011; p 165.
(67) *NIST Critical Stability Constants of Metal Complexes*, Version 8; National Institute of Standards and Technology: Washington, DC, 2004.
(68) Sansonetti, J. E.; Martin, W. C.; Young, S. L. Handbook of Basic Atomic Spectroscopic Data. *J. Phys. Chem. Ref. Data.* **2005**, *34*, 1559−2259. *NIST Physical Data Web Site* <http://www.nist.gov/pml/data/handbook/index.cfm > (December 2012).
(69) Loh, S. K.; Hales, D. A.; Lian, L.; Armentrout, P. B. Collision-Induced Dissociation of Iron Cluster Ions (1^+) (Fe_n^+) (n = 2−10) with Xenon: Ionic and Neutral Iron Binding Energies. *J. Chem. Phys.* **1989**, *90*, 5466−5485.